PFC/JA-90-29

Fast Wave Ion Cyclotron Resonance Heating Experiments on the Alcator C Tokamak

T. D. Shepard*, C. L. Fiore,
F. S. McDermott†, R. R. Parker, M. Porkolab

Plasma Fusion Center
Massachusetts Institute of Technology
Cambridge, MA 02139

August, 1990

To be published in Physics of Fluids

This work was supported by the U. S. Department of Energy Contract No. DE-AC02-78ET51013. Reproduction, translation, publication, use and disposal, in whole or in part by or for the United States government is permitted.

Fast Wave Ion Cyclotron Resonance Heating Experiments on the Alcator C Tokamak

T. D. Shepard*, C. L. Fiore, F. S. McDermott† , R. R. Parker, M. Porkolab

Plasma Fusion Center,
Massachusetts Institute of Technology,
Cambridge, Massachusetts 02139, USA

Abstract

In this paper, minority regime fast wave ICRF (Ion Cyclotron Range of Frequency) heating experiments conducted on the Alcator C tokamak are described. Up to 450 kW of RF (Radio Frequency) power at frequency $f = 180$ MHz was injected into plasmas composed of deuterium majority and hydrogen minority ion species at magnetic fields of $B_0 \simeq 12$ T, densities $0.8 \leq \bar{n}_e \leq 5{\times}10^{20}\,\mathrm{m}^{-3}$, and minority concentrations $0.25 \lesssim \eta_H \leq 8\%$. Typical ion temperatures were $T_D(0) \sim 1$ keV, while, depending on density, typical electron temperatures were in the range $T_e(0) \sim 1.5$–2.5 keV. Central deuterium ion temperature increases of $\Delta T_D(0) = 400$ eV were observed at $\bar{n}_e = 1 \times 10^{20}\,\mathrm{m}^{-3}$, while significantly smaller ion temperature increases were observed at higher densities. At the highest densities, ion heating became insignificant due in part to a limitation on power handling by the antenna that became more severe with increasing density. Significant electron heating was not observed at any density. Heating of the minority species at low densities indicated severe losses, but at higher densities it was consistent with efficient collisional coupling of the RF power from the hydrogen minority species to the deuterium majority species. Analysis of the deuterium power balance indicated no significant change in the deuterium thermal transport properties as a function of RF power. This may be consistent with the fact that the RF power never exceeded the Ohmic heating (OH) contribution. However, a very strong dependence of the deuterium transport properties on density was observed, and appears to be the dominant process limiting the effectiveness of ICRF heating at high density.

I. Introduction

The work described in this paper is concerned with auxiliary plasma heating using RF power in the ion cyclotron range of frequencies (ICRF) in the compact, high-magnetic-field tokamak Alcator C. The distinguishing characteristics of this work are the unprecedented high electron densities and magnetic fields at which the experiments were carried out and the emphasis on ion energy transport in the data analysis. ICRF heating has been successfully tested in tokamaks at relatively low densities, $\bar{n}_e < 1 \times 10^{20}\,\mathrm{m}^{-3}$. [1, 2] For the work described herein, the primary concern is the scaling of ICRF heating results to significantly higher densities. Previous attempts at ICRF heating in Alcator A [3] and Alcator C have been somewhat disappointing [4–6], although improved heating efficiency was observed during ion Bernstein wave heating experiments[7], which were conducted in parallel with the fast-wave experiments described herein.

The majority ion species in these experiments was always deuterium and the minority species was always hydrogen, resulting in a required toroidal magnetic field of 12 T for hydrogen fundamental (or deuterium second harmonic) absorption at the available generator frequency of 180 MHz.

The compact nature of the Alcator tokamak imposes severe limitations on the design of the ICRF launcher, and the previous ICRF experiments on Alcator C were restricted to using relatively narrow antennas and therefore non-optimal $N_{\|}$ spectra. One of the goals of the present work was to improve the design of the RF system, to allow injection of the total available ICRF power ($\sim$ 400 kW) for long pulse-lengths (100 ms or more) without electrical arcing in the antenna or transmission line. In the present experiments a double-strap antenna was used to produce a narrower $N_{\|}$ spectrum than in the previous experiments, and hence improved coupling and wave penetration.

To explain the experimental results, a modeling effort was undertaken to study the physics of wave propagation and absorption, and related energy transport. By concentrating the study on the behavior of the deuterium heating, we calculate the net power transferred to the deuterium through collisional exchange with the minority hydrogen species

and direct deuterium second-harmonic absorption from the RF waves. Subsequently we compare this with the collisional-exchange power to deuterium from electrons (calculated directly from experimental density and temperature measurements). We find that, as far as the deuterium is concerned, the heating efficiencies of the deposited RF power and the electron-ion collisional exchange power are equal. Specifically, the deuterium responds to the heating power as if there were no change in the ion thermal transport properties during RF power injection.

However, to explain the observed minority temperatures at low densities ($\bar{n}_e \sim 1 \times 10^{20}\,\mathrm{m}^{-3}$), the hydrogen minority species must be subject to severe losses, and significant electron heating was not observed at any density. It was not possible to obtain data related to electron loss mechanisms during the limited operating period, but the lack of electron heating is consistent with the weak minority heating and an influx of high-Z impurities (the resistive loop voltage always increased during RF injection). It should be noted that the limiters and antenna Faraday shield surfaces were made of molybdenum. In earlier fast wave ICRF heating experiments on Alcator C the limiters were graphite but the Faraday shield, vacuum vessel wall and limiter support structures were all stainless steel[4]. A study of impurity radiation was undertaken by Manning, et al [5, 6]. It was found that radiation from high-Z impurities was significantly reduced during the Ohmic phase of the discharge, but still dominated during RF injection.

To explain the experimental results at high density, it is not necessary to postulate any additional loss mechanism associated with the RF absorption for any charged particle species. The weak deuterium heating observed as density is increased is consistent with an unfavorable scaling to high density of the ion thermal confinement.

The behavior of ion conductivity versus density found in the present study was also observed in the ion Bernstein wave heating experiments carried out by Moody, et al.[7], where a better density variation at fixed plasma current was achieved during the scan, and also in previous non-ICRF Alcator C experiments reported[8-10], where the variation in confinement versus plasma current was emphasized during the analysis. It has been suggested as the mechanism responsible for the so-called saturated confinement regime in

which energy confinement progressively degrades compared to neo-Alcator scaling ($\tau_E \propto \bar{n}_e$) with increasing density in the range $\bar{n}_e \gtrsim 3 \times 10^{20}\,\mathrm{m}^{-3}$. The physical argument put forth to explain the results was that ion confinement degradation with increasing density combined with increased collisional coupling between ions and electrons increases the electron energy "loss" channel.

During pellet injection experiments performed using high-density target plasmas in the saturated confinement regime[8], it was found that pellet injection resulted in a significant improvement in energy confinement time. The post-injection plasmas had energy confinement times consistent with a decrease in the ion thermal diffusivity to the neoclassical value ($W_{\mathrm{neo}} = 1$). However, at those high densities the electrons and ions are so strongly coupled collisionally that it is not possible to determine unambiguously whether the improvement was a result of suppression of anomalous ion losses or of improved electron confinement. To resolve this ambiguity, further experiments were performed at moderate density ($1 \times 10^{20}\,\mathrm{m}^{-3} \leq \bar{n}_e \leq 3 \times 10^{20}\,\mathrm{m}^{-3}$).[10] For this density range, which is the same range used for the ICRF analysis in the present work, the electron and ion temperatures are separated sufficiently that the loss channels could be distinguished. Using the ONETWO transport analysis code[11], Wolfe et al. determined unambiguously that the ion thermal diffusivity was reduced to the neoclassical value following pellet injection. Wolfe et al. suggested that the ion-temperature-gradient-driven mode[12-16], or η_i-mode, may have been responsible for the deteriorated ion confinement at high densities in Alcator C.

The remainder of this paper is organized as follows: In Sec. II, a brief description of the ICRF fast-wave antennas used in these experiments is given. In Sec. III, experimental results are presented for relatively low-density Alcator C discharges. In Sec. IV, results are presented for a density scan in which the density was increased until the observed heating became experimentally insignificant. In Sec. V, the deuterium power balance is examined in detail with the aid of numerical simulations. The summary and conclusions are presented in Sec. VI.

II. ICRF Fast-Wave Antennas

Two different ICRF antennas were used during these experiments, and are illustrated in Fig. 1. The design of these antennas was determined by the physical constraints imposed by the compact dimensions of the tokamak. Each antenna consists of a two-element toroidal array, with the elements fed in parallel and in phase by a single coaxial line. There was no provision for adjusting the phase between antenna conductors. Since the access port in the tokamak is only 4 cm wide, each antenna consists of two 4 cm-wide modules which were assembled inside the vacuum chamber. Each module consists of a radiating conductor shorted to the backplane at each end, and covered by a double-layer Faraday shield. All antenna parts are machined from stainless steel. The antenna current straps are plated with silver, and the Faraday shield outer surfaces were coated with a 0.018 inch-thick layer of molybdenum. The two-side-launch antenna was self-resonant, and was fed in such a manner as to produce a nominally matched load to the transmission line, while the outside-launch antenna was a simple, center-tapped electrically short loop. Reflected power was maintained typically below 3% in each antenna. Double-stub tuning was used to match the low-field-side launch antenna to the transmission line. For fine-tuning of the match for the two-side launch antenna, eliminating reflections from the vacuum feedthrough, and to provide a match during vacuum conditioning, a single stub plus phase shifter were used. Owing to the high antenna loading provided by the high-density Alcator C plasmas, it was particularly easy to maintain a very good match without the need for automatic tuning. Based on the ratio between vacuum and plasma loading, resistive losses in the antenna were estimated to be typically $\sim$ 5%, a negligible amount. No significant differences in the experimental results were observed with either of these two antennas. Due to source limitations, only one antenna was powered at a time. Further details of the antenna design can be found in Ref. 17.

III. Low-Density Experimental Results

Typical plasma parameters are shown in Table I, during the Alcator C ICRF and Ohmic experiments. To provide space for the antennas inside the vacuum chamber, it was necessary to reduce the minor radius of the plasma from 16.5 cm to 12.5 cm by installing special limiters. It was not possible to vary the plasma current independently of the density during the ICRF experiments. A plasma current of $I_P = 140$ kA was typical at the lowest plasma density ($\bar{n}_e \simeq 1 \times 10^{20}\,\mathrm{m}^{-3}$), and $I_P = 410$ kA was typical during the high density discharges ($\bar{n}_e \simeq 5 \times 10^{20}\,\mathrm{m}^{-3}$). With very few exceptions, the variation of plasma current for intermediate densities was approximately a linear extrapolation between these two values. The central electron temperature, determined from the YAG (Yttrium Aluminum Garnet) laser Thomson scattering system[18], was ~ 2.5 keV at low density and decreased to ~ 1.5 keV at high density, while the deuterium ion temperature was ~ 1 keV at low density, increasing to ~ 1.3 keV at high density. The Ohmic heating power increased from ~ 200 kW to ~ 1 MW as density increased.

At relatively low densities ($0.8 \lesssim \bar{n}_e \lesssim 1.5 \times 10^{20}\,\mathrm{m}^{-3}$) the heating results were somewhat comparable to results from early minority regime experiments carried out on the TFR (Tokamak Fontenay-aux-Roses) tokamak[19]. Data from two such discharges are shown in Figs. 2 and 3, and in Tables II and III. A change in plasma density was sometimes observed to occur during RF power injection, as shown in Fig. 2. Since the deuterium temperature was always less than the electron temperature, even during the RF heating phase, the increased collisional coupling between electrons and deuterium during rising-density discharges is expected to contribute to the deuterium heating. For the rising-density discharge in Fig. 2, the deuterium temperature measurement from the charge-exchange neutral energy analyzer indicates $\Delta T_D(0) = 400$ eV for $P_{\mathrm{RF}} = 300$ kW while for the steady-density discharge shown in Fig. 3, the deuterium temperature deduced from the neutron rate indicates $\Delta T_D(0) = 175$ eV for $P_{\mathrm{RF}} = 220$ kW. The charge-exchange diagnostic can only measure the temperature of one ion species during a discharge. Therefore, due to the need to use the charge-exchange diagnostic for monitoring the minority species, it was often

necessary to rely on the neutron diagnostic for determining the deuterium ion temperatures. The resistive loop voltage was always observed to increase during RF heating. This is evidently a result of the lack of electron heating and an influx of high-Z impurities (no carbonization was used during these experiments and the limiters and Faraday shield surfaces were made of molybdenum). Thomson scattering data for a typical low-density discharge, indicating no discernable electron heating, are shown in Fig. 4.

The dependence of the hydrogen minority tail temperature on minor radius was determined from the charge-exchange diagnostic by scanning the viewing chord in the vertical direction during a series of similar discharges. (It was not possible to view tangentially with the charge-exchange diagnostic in Alcator C due to the restricted diagnostic port access.) Data from this scan are shown in Fig. 5 for minor radii up to 7 cm. It is not possible to obtain accurate measurements for larger minor radii due to the influence of wall reflections on the charge-exchange measurement. Also shown are the deuterium majority temperatures, which were also obtained from the charge-exchange diagnostic. Two consecutive discharges were taken at each viewing angle and one ion species was measured on each discharge. The minority concentration $\eta_H \equiv n_H/(n_H + n_D)$ is estimated from the hydrogen and deuterium flux measured by neutral particle anlysis to be only 0.5% for these discharges (the mass rejection of this instrument is 1000:1). Other parameters for this series of discharges are shown in Table IV. For these discharges, there was a slight drop in density during RF injection. The RF power was typically $P_{\rm RF} = 250$ kW which yielded a central deuterium temperature rise of $\Delta T_D(0) = 140$ eV. The central deuterium temperature was monitored using the neutron diagnostic when the charge-exchange analyzer was not viewing along a central chord.

From these data, one can estimate the collisional exchange power P_{HD} from the hydrogen minority to the deuterium majority. Assuming the density profile to be a parabola and the hydrogen distribution function to be a Maxwellian with the temperature profile indicated in Fig. 5 P_{HD} is found to be 8 kW (including only the region $r \leq 7$ cm for which data were available), in stark contrast to the $P_{\rm RF} = 250$ kW that was launched. This collisional-exchange-power radial profile is approximately uniform within the minor radii $r \leq 7$ cm for which data are available. From Fokker-Planck calculations (similar to those

described later in this paper) including the entire minor-radial cross section $r \leq 12.5$ cm, we obtain $P_{HD} = 15$ kW. From the RF wave absorption calculations, also described later in this paper, we determine the direct deuterium second-harmonic absorption to be also $P_D = 15$ kW, but with a significantly more centrally peaked profile. Thus, deuterium second harmonic absorption is probably the dominant source of central heating for these discharges.

As demonstrated in Fig. 6, the most efficient deuterium heating was observed at the lowest possible minority concentration $\eta_H \lesssim 0.5\%$. (Other parameters for this series of discharges are shown in Table V.) The most efficient hydrogen fundamental absorption (i.e., wave damping) is expected when the quantity $n_H|E_+|^2$ is maximized[20]. (Here E_+ is the left-hand circularly polarized component of the poloidal RF electric field with respect to a stationary observer viewing along the direction of the equilibrium magnetic field.) For Alcator C parameters, this yields an optimum minority concentration of $\eta_H \sim 2\%$. If one postulates some kind of parasitic loss mechanism — large resistive antenna losses or direct absorption in the plasma edge due to inefficient wave launching, for example — then the above calculation is still relevant, and one expects the most efficient deuterium heating at $\eta_H \sim 2\%$. This is true as long as most of the RF power that reaches the deuterium is channeled first through the hydrogen, regardless of the loss mechanisms present. If one assumes that the deuterium distribution function is Maxwellian, then there is also a small contribution from direct deuterium second harmonic absorption given by $P_D \approx (\beta_D/\eta_H) \times P_H$, which corresponds approximately to 5% of the coupled power for typical Alcator C parameters. For the small values of P_D involved, Fokker-Planck calculations[17] show that the resulting non-thermal deuterium tail would be insignificant and that most of the deuterium absorption would take place on the bulk of the deuterium distribution function. Indeed, the experimentally measured deuterium charge-exchange spectrum, an example of which is shown in Fig. 7, exhibits no evidence of a non-thermal tail. As discussed later in Sec. V of this paper, in the calculations it will be assumed that minority ions are not confined if their energy is higher than a critical value E_{Loss}, which is determined by toroidal-field ripple-trapping. In Alcator-C the field errors on axis are relatively large.[21] At high densities this is not a significant effect due to the rapid collisional equilibration of the

hydrogen minority species. But at low densities so much of the power absorbed by hydrogen is lost through this mechanism that the amount P_{HD} remaining no longer dominates over the second-harmonic contribution P_D. Thus, we believe that the RF power is being efficiently absorbed, but that a large amount of power is lost due to poor confinement of the hydrogen minority species in the lower-density plasmas.

IV Results of Experimental Density Scan

The observed central deuterium temperature increase $\Delta T_D(0)$ is plotted as a function of density $\bar{n}_e$ in Fig. 8 for every discharge in the database. Deuterium heating was observed for densities up to $\bar{n}_e \sim 5\times10^{20}\,\mathrm{m}^{-3}$. The RF power corresponding to the highest values of ΔT_D was $P_{\mathrm{RF}} \sim 300$ kW for $0.8 \leq \bar{n}_e \lesssim 2\times10^{20}\,\mathrm{m}^{-3}$. For higher densities, the maximum power that could be injected without breakdown on the antenna surface decreased with increasing density to $P_{\mathrm{RF}} \sim 175$ kW at $\bar{n}_e \sim 5\times10^{20}\,\mathrm{m}^{-3}$.

Although most of the experiments were performed with $P_{\mathrm{RF}} \lesssim 300$ kW, power levels as high as 500 kW, limited only by available generator capacity, were achieved for $1 \lesssim \bar{n}_e \lesssim 2\times 10^{20}\,\mathrm{m}^{-3}$. Including a peaking factor of 2 due to the electrical length of the antennas, 500 kW would correspond to a maximum power density of approximately 4 kW/cm^2 at the antenna surface. Hence the power density limit during the density scan decreased from 2.5 kW/cm^2 (not actually at the limit) to 1.4 kW/cm^2 as density increased to $\bar{n}_e \sim 5\times10^{20}\,\mathrm{m}^{-3}$. However, we also found the same total power limits in earlier experiments using a single-element antenna, for which the corresponding power densities would be double. Although the antenna voltage was not measured directly during these experiments, we suspect, based on electrical models for the antennas, that the power limit is more directly related to the antenna voltage than to the actual coupled power. (The inductance and capacitance of the single-element antenna were not the same as for the double-element antennas.) This problem merits more investigation considering its importance for future devices.

The energy confinement time $\tau_E = W/P$ and the incremental energy confinement time $\tau_{\mathrm{inc}} = \Delta W/\Delta P$ are plotted in Fig. 9. Here W is the total thermal energy content of

the plasma (all species) and P is the total power input to the plasma (Ohmic plus RF). The incremental confinement time exhibits a great deal of scatter and shows no obvious density scaling. However, it is clear from Fig. 9 that the efficiency of the RF heating is significantly less than that of the Ohmic heating, whose efficiency increases with density. For the low-density range, this can be understood in terms of poor confinement of the hydrogen minority. But this does not explain the degraded heating efficiency at high density, where confinement of the minority ion species is not an issue.

Finally, the calculation of Z_{eff} from the resistive loop voltage, as determined by the ONETWO code[11] (discussed below), is shown in Fig. 10. Normally, Z_{eff} for Alcator C is determined from a diagnostic which measures visible bremstrahlung radiation[22], but that diagnostic was seriously affected by RF interference during the experiments. Therefore, the measurement in Fig. 10 is the best Z_{eff} measurement available for these discharges. A few comparisons were made with the visible bremstrahlung measurement, by looking at the value of Z_{eff} indicated immediately after the RF turned off, and no significant disagreement was found. There is a tendency for significant increase of Z_{eff} during the RF power injection, although high-density discharges are less susceptible to this effect, due in part to lower RF power levels at the highest densities.

V Deuterium Power Balance

To understand the scaling of the RF heating efficiency with density, it is helpful to perform an analysis which concentrates more closely on the power sources and energy confinement of the deuterium, in isolation from the other plasma components. That is, we treat the hydrogen and electrons as known sources of collisional exchange power to the deuterium, add in the contribution from direct deuterium second harmonic absorption, and then model the various loss mechanisms of the deuterium. The procedure that is being suggested is outlined in Fig. 11, which also serves to define the terminology used in the following discussion. The goal is to account for the power deposited on the deuterium by determining the sources P_D (deuterium second-harmonic absorption), P_{HD} (collisional exchange between minority hydrogen and majority deuterium), and P_{eD} (collisional exchange between electrons and deuterium), and balancing them against losses due to deuterium energy transport via convection, conduction, and charge-exchange.

The only quantities in Fig. 11 which can be determined directly from experimental data are $P_{\rm RF}$ and $P_{\rm OH}$. (It is the lack of temperature profile measurements that is responsible for the inability to directly calculate the collisional exchange powers.) It is necessary to rely on numerical modeling to obtain estimates for the remaining quantities.

Two separate computer programs were used to separate $P_{\rm RF}$ into P_H (hydrogen fundamental cyclotron absorption), P_D, and $P_{\rm MC}$ (mode-conversion of the fast wave to the ion Bernstein wave). One program is a 1D 6th-order full-wave code originally developed by Brambilla[23] to model coupling by ICRF antennas, particularly for launching ion Bernstein waves. This code can treat a slab plasma bounded by conducting walls with an antenna near one wall, and yields values for P_H, P_D, and $P_{\rm MC}$. However, a 1D code obviously does not treat the geometry properly and cannot yield reliable radial profile information. The other program is a 2D 2nd-order full-wave code developed by Smithe and Colestock[24]. This code uses a reduced-order dielectric wave operator which results in mode-converted power appearing as additional dissipation. Essentially, this code yields radial profile information for the quantities P_H and $P_D + P_{\rm MC}$. The quantities $P_D + P_{\rm MC}$ calculated from each of these codes agree well with one another except for cases with high minority concentration.

Regarding absorption of the ion Bernstein wave (IBW), the Brambilla code calculates IBW absorption on electrons, but this is always quite negligible for Alcator C parameters. The code also assumes stochastic damping of the IBW at large $k_\perp \rho_i$, which occurs near the plasma edge on the high-magnetic-field side. In the Smithe-Colestock code, mode conversion appears as absorption at the point where the mode conversion occurs. This would be a reasonable approximation only in cases where the IBW was very strongly damped (or where mode-conversion was very weak), which is not usually the case in Alcator C.

Other calculations[17] were done using the 1D, full-wave, single-pass codes METS and CARDS[25]. These codes perform the same calculation as the original Colestock-Kashuba code[26]. These calculations also indicate that IBW absorption is very weak for typical Alcator C plasmas. Therefore, in the following treatment, mode-converted power will be assumed to be lost (presumably at the plasma edge).

The hydrogen power balance was analyzed using the time-dependent bounce-averaged Fokker-Planck code FPPRF[27]. This code solves the drift-kinetic equation for the hydrogen minority with a Coulomb collision operator, an RF quasilinear diffusion operator, and various non-ideal loss terms included. The non-ideal effects included are neoclassical transport, unconfined orbit losses, asymmetric drag, toroidal-field ripple diffusion, and charge-exchange losses. A term is also included which maintains the minority concentration at a specified value regardless of the various loss processes present. One problem that was encountered when using this code is that the toroidal-field ripple diffusion operator used is inaccurate when trapping in finite magnetic wells is significant since the field ripple is localized at port locations. This results in a significant over-estimate of the minority temperature, under-estimate of the loss P_{Loss}, and over-estimate of P_e. However, the calculation of P_{HD} and its radial profile are still believed to be approximately correct. This was shown to be true by introducing an ad-hoc loss into the calculation which lowered the energy E_{Loss} at which the minority ions became unconfined. The calculation of P_{HD} is not sensitive to the value of E_{Loss} so long as $E_{\text{Loss}} > E_{\text{crit}}$ where E_{crit} is the energy at which the ion drag and electron drag terms are equal for a minority ion.

The electron power balance was not analyzed. Instead, the electron temperature profile was determined via a well-known procedure in which the electron temperature profile

is related to the current profile by assuming classical resistivity, the current profile is related to the poloidal field profile through the Ampere equation, and then the poloidal field profile is adjusted to match the central and surface values of the MHD (Magnetohydrodynamic) safety factor.[17]The central electron temperature is measured by Thomson scattering and the peak of the profile is adjusted to match this value. The collisional exchange power P_{eD} is then computed by the ONETWO code, which is used to analyze the deuterium power balance. This procedure effectively bypasses uncertainties in P_e, the contribution from the mode-converted ion Bernstein wave, and the effects of impurity radiation.

The calculation of the power $P_{\rm Net} = P_D + P_{HD}$ for a six-point density scan is summarized in Fig. 12. Here $P_{\rm Net}$ is the net power deposited to deuterium as a result of the RF power injection (not including changes in P_{eD}). At low density, the losses are due primarily to unconfined orbits and ripple trapping, whereas at high density the losses are primarily due to mode-conversion. The total fraction of the RF power deposited on deuterium increases from 13% at $n_{e0} = 1 \times 10^{20}\,\mathrm{m}^{-3}$ to 53% at $n_{e0} = 6 \times 10^{20}\,\mathrm{m}^{-3}$. Moreover, the $P_{\rm Net}$ profile shape becomes increasingly more favorably peaked with increasing density. Thus, the effect of increasing density on RF absorption is very favorable and cannot explain the behavior exhibited in Figs. 8 and 9.

The same calculation for a seven-point minority-concentration scan is shown in Fig. 13. For reasons discussed in detail in Ref. 17, we were not able to obtain results from the FPPRF code for $\eta_H > 2\%$. We may conclude that if the mode-converted power does not contribute significantly to deuterium heating, then it is the large increase in mode-converted power with increasing η_H that is responsible for the monotonic decrease of the experimental heating efficiency with increasing η_H. Physically, this is a result of the increasing distance between the cyclotron resonance layer and the mode-conversion layer with increasing η_H, combined with the low minority temperatures resulting from the strong collisional coupling of RF power from the hydrogen to the deuterium at high minority concentration. That is, there is not sufficient Doppler-broadening of the cyclotron resonance for the cyclotron and mode-conversion layers to overlap[2]. Since single-pass absorption is low for these plasmas, mode-conversion then dominates. However, apparently the mode-converted waves are not absorbed directly by the electrons or ions in the bulk of the plasma.

Having arrived at estimates for the RF deposition on deuterium, $P_{\rm net}$, it is then possible to analyze the deuterium power balance. This was done using the ONETWO transport code[11]. In this analysis, the electrons, hydrogen, and ICRF are treated as known sources of heating power for the deuterium (P_{eD}, P_{HD}, and P_D respectively). Then, several loss mechanisms associated with energy transport are examined. The energy balance equation solved in these ONETWO runs is

$$\frac{3}{2}\frac{\partial}{\partial t}(n_D T_D) = \frac{1}{r}\frac{\partial}{\partial r}\left[r\left(n_D \chi_D \frac{\partial T_D}{\partial r} - \frac{5}{2} T_D \Gamma_D\right)\right] - \frac{\Gamma_e}{n_e}\frac{\partial}{\partial r}(n_D T_D) - P_{\rm CX} + P_{eD} + P_{\rm dep} \qquad (1)$$

in which the rate of change of the deuterium thermal energy is balanced against thermal conduction, convection, the work done on the ions by the electrons as they flow against the ion pressure gradient, charge-exchange loss ($P_{\rm CX}$), collisional exchange with electrons (P_{eD}), and the net deposition of RF power on deuterium ($P_{\rm dep}$). The electron flux Γ_e is determined from the equation

$$\frac{\partial n_e}{\partial t} + \frac{1}{r}\frac{\partial}{\partial r}(r\Gamma_e) = S_e \qquad (2)$$

where S_e includes the effects of ionization and recombination of impurities. The electron source rate S_e is calculated via a neutral transport package which is included as a subsystem in ONETWO. The boundary condition for this calculation is derived from an assumed global particle confinement time, but the results of these analyses are insensitive to the exact choice of this parameter. A single impurity species is allowed in ONETWO, which was taken to be oxygen in the calculations presented here. Impurity transport is treated kinetically. The ion flux Γ_D is then determined from ambipolarity. For all of the cases analyzed, the conduction, electron collision, and RF deposition were the dominant terms. The convection, charge exchange, and work, though insignificant, were included in the calculations.

All the source and loss terms in Eq. (1) were evaluated according to the models just described, using experimental data. For each experimental discharge that was analyzed, the evaluation was performed as a function of time, both during the Ohmic and RF heated

portions of the discharge, and the results were evaluated for consistency with and without RF power. The experimental parameters used as input to the code are the electron temperature $T_e(r,t)$, electron density $n_e(r,t)$, toroidal field B_0, toroidal current $I_P(t)$, resistive loop voltage $V_R(t)$, fusion neutron production rate $R_f(t)$, and an assumed value of the central safety factor $q_0(t)$ (unity or slightly less depending on whether sawteeth were evident in the central soft x-ray signal). The central electron temperature was taken from Thomson scattering data, and the profile shape was determined using the model discussed above. The electron density profile was determined by fitting a parabola raised to an adjustable power to the central density from Thomson scattering and the line-average density from the interferometer. The ion temperature and profile shape, and the current density profile shape were determined automatically and self-consistently by ONETWO. The impurity charge state was determined from coronal equilibrium using the specified electron temperature, and the deuterium density was calculated from charge neutrality. Finally, both the central deuterium temperature and the deuterium temperature profile were determined by solving the ion heat transport equation (Eq. (1)) assuming an ion thermal diffusivity of the form

$$\chi_D = W_{\rm neo}\chi_D^{CH} + D_b f(q) \tag{3}$$

where χ_D^{CH} is the Chang-Hinton neoclassical diffusion coefficient[28, 29], which is multiplied by an adjustable scale factor $W_{\rm neo}$, D_b is the Bohm diffusivity and

$$f(q) = \begin{cases} 1 - \frac{1}{1+(1/q-1)^2}, & q \le 1 \\ 0, & q > 1 \end{cases} \tag{4}$$

models the time-averaged effect of sawtooth activity. The contribution from D_b was found to be completely negligible in all cases studied. The neoclassical multiplier $W_{\rm neo}(t)$ is adjusted dynamically so that a fusion neutron production rate calculation matches the experimental measurement. The electron-deuterium collisional exchange power was determined classically, from the expression

$$P_{eD} = \frac{3}{2} n_e \nu_{eD} (T_e - T_D) \tag{5}$$

where

$$\nu_{eD} = \frac{8\sqrt{\pi}}{3} \frac{m_e}{m_D} \left(\frac{e^2}{4\pi\epsilon_0} \right)^2 \frac{\lambda n_D}{\sqrt{m_e} T_e^{3/2}} \tag{6}$$

and the RF deposition to deuterium was calculated as described above.

The parameter adjustments discussed in the preceeding paragraph are done by ONETWO using a PD (proportional-differential) feedback law in real time (i.e., transport time). The neoclassical multiplier $W_{\rm neo}$ is adjusted by comparing the calculated fusion neutron rate and its time derivative with the specified input value. The central and edge values of $Z_{\rm eff}$ are adjusted by comparing the values of resistive loop voltage and central safety factor and their time derivatives with the specified input values. The resistive loop voltage and central safety factor are determined from the current and resistivity profiles calculated in the code. The resistivity is calculated neoclassically, including corrections due to banana-trapped particles. Then the electric field and current profiles are determined from the magnetic diffusion equation.

It is possible for ONETWO to experience some difficulty when adjusting parameters dynamically to match input specifications. This tended to occur often in the runs at the time when the RF turns on and parameters try to change quickly. Due to temporary inconsistencies in the input data, due in particular to the 20-ms intervals between Thomson-scattering data points, ONETWO would make inappropriate adjustments in the neoclassical multiplier but would subsequently recover. Data determined to be affected by this effect are indicated by broken lines in Fig. 14.

The ONETWO analysis was performed for 44 discharges from the experimental database. These 44 discharges include a variety of minority concentrations (mostly $\eta_H = 0.5\%$ plus the discharges from the η_H-scan up to $\eta_H = 2\%$), and a variety of RF powers $175 \leq P_{\rm RF} \leq 350$ kW, as well as discharges with density rising, steady, and falling during RF power injection. The results for three representative discharges are shown in Fig. 14. Case (a) is a relatively low-density discharge in which the density increased from $\bar{n}_e = 1.35 \times 10^{20}\,{\rm m}^{-3}$ to $\bar{n}_e = 1.53 \times 10^{20}\,{\rm m}^{-3}$ during RF power injection. Case (b) is a medium-density discharge in which the density decreased from $\bar{n}_e = 1.8 \times 10^{20}\,{\rm m}^{-3}$ to $\bar{n}_e = 1.6 \times 10^{20}\,{\rm m}^{-3}$ during RF power injection. And case (c) is a high-density discharge in which the density was relatively constant during RF power injection, decreasing only slightly from $\bar{n}_e = 2.95 \times 10^{20}\,{\rm m}^{-3}$ to $\bar{n}_e = 2.8 \times 10^{20}\,{\rm m}^{-3}$. Values which have been

determined to be erroneous due to failure of ONETWO to match the input value (usually of the fusion neutron rate) are shown with broken lines. For each of the three discharges in Fig. 14, the resulting value of W_{neo} is plotted as a function of time for three different values of the P_{dep} term in Eq. (1). Each case was run three times, assuming the power deposited to deuterium to be zero, P_{net} from the calculations described above, and the total launched power P_{RF} respectively. For the $P_{\mathrm{dep}} = P_{\mathrm{RF}}$ cases, the RF power was assumed to be uniformly distributed for $r < a/2$, and zero for $r > a/2$.

When it is assumed that no RF power is deposited to deuterium, a noticeable drop in the calculated value of W_{neo} occurs during RF power injection. This behavior was observed for all 44 of the discharges that were analyzed, regardless of whether or not there was any change in profile shapes, and regardless of whether the density increased, decreased, or remained relatively constant during RF power injection. Therefore we conclude that some amount of RF power must have been absorbed by the deuterium species to produce the observed deuterium heating. If the RF power deposition model described above is used, the resulting values of W_{neo} remain reasonably constant throughout the discharge. If all of the RF power is assumed to be deposited on deuterium, then the inferred value of W_{neo} always increases significantly during RF power injection.

The behavior of the neoclassical multiplier W_{neo} as well as the values of the actual thermal conductivity κ at $r = a/2$ are shown in Fig. 15 for all 44 of the discharges that were analyzed. These values were calculated using the value of $P_{\mathrm{dep}} = P_{\mathrm{net}}$ from the preceding calculations. An explanation for the unfavorable scaling of the RF heating efficiency with density now begins to appear. For the Ohmic target plasma, the deuterium thermal energy transport is nearly neoclassical at low density, but becomes increasingly anomalous with increasing density. Moreover, the observed deuterium heating is consistent with no significant change in the thermal transport properties during RF heating, in spite of the fact that the net RF deposition from the estimates developed herein increases significantly with density. In other words, after accounting for known RF loss mechanisms according to theoretical models, the net RF power deposited to deuterium heats with the same efficiency as the net Ohmic power deposited via collisional exchange with electrons.

It should be emphasized that the effect of increasingly anomalous ion conductivity is a significant effect compared to the neoclassical prediction. The data in Fig. 15 exhibit an extra factor of n dependence compared with neoclassical transport. All plasmas that were analyzed were in the plateau regime of neoclassical transport for $r = a/2$. In the plateau regime, χ^{CH} is not strongly dependent on density, so that $\kappa^{CH} = n\chi^{CH}$ is proportional to n. In our data we have $\kappa \propto n^2$ which, incidentally, is the density dependence exhibited in the banana neoclassical regime. Another coincidence which we observe is that if one extrapolates the data in Fig. 15 to the point where $W_{\rm neo} = 1$, this occurs at the boundary between the plateau and banana regimes.

Another way to compare the effectiveness of Ohmic and RF heating of the deuterium is to directly compare the net RF power deposited on deuterium with the collisional exchange power from electrons. (This less precise comparison glosses over differences in RF and Ohmic power deposition profile shapes.) Such a comparison is shown in Fig. 16. The total ion heating power is shown both before and during the RF power injection. The split between the collisional exchange and the RF deposition is also shown. Changes in the convection, work, and charge exchange (which are small to begin with) are insignificant, but the collisional exchange power decreases significantly during the RF heating phase, due to the decrease in the temperature difference between electrons and deuterium as the deuterium heats up. However, the total ion heating power does not change significantly. Thus, the main effect on the deuterium of applying RF power to the Alcator C target plasma is a replacement of collisional exchange power with RF power.

We now offer the following physical explanation for the results of the experimental density scan. First, we remark that the RF confinement time and incremental confinement time in Fig. 9 were calculated assuming that all the generated RF power was deposited to the plasma without loss. Also, these confinement times are global quantities including the effects of both electrons and ions, while it was only the ions which were heated. If these confinement times were re-calculated using the quantity $P_{\rm Net}$ from the simulations, then all the RF confinement times would increase, with the largest increases being at low density. One would then have effectively the same information as is contained in Fig. 15. At low density, the deuterium thermal confinement is superior to that of the electrons

and the deuterium is weakly coupled collisionally with the electrons. Thus, although only a small amount of the RF power is deposited to deuterium, there is a relatively large amount of heating. As the density increases, while the electron thermal confinement is improving (neo-Alcator scaling) the deuterium thermal confinement is degrading. Thus heating the deuterium becomes less effective at high density, in spite of the fact that RF absorption and thermalization are improving. But if one looks at the power balance of just the deuterium, the power absorbed from the RF source and the power absorbed from Ohmic heating (P_{eD}) heat with equal effectiveness.

In conclusion, regardless of the cause of this anomalous ion confinement, the resulting values of $W_{\rm neo}$, which are very similar in the present ICRF experiments to those found by Wolfe et al., are sufficient to explain the observed density scaling of the ICRF heating efficiency. We emphasize that, while anomalous ion confinement is very commonly observed in tokamak plasmas, what is unique about Alcator C plasmas is that the ions are not anomalous at low density. As density increases, the ion transport becomes progressively anomalous. Unless one attempts a very sophisticated data analysis, this variation in ion energy transport can mask the expected increase in ICRF heating efficiency with increasing density.

VI Summary

Results from fast-wave ICRF heating experiments conducted on the Alcator C tokamak with metallic limiters and Faraday shields have been presented and analyzed. Although significant deuterium and hydrogen heating was observed, in general electron heating was not found. At relatively low densities ($0.8 \lesssim \bar{n}_e \lesssim 1.5 \times 10^{20}\,\mathrm{m}^{-3}$) the hydrogen tail temperatures were too low to account for more than a small fraction of the injected RF power. In contrast to theoretical expectations, the heating was most efficient at the lowest obtainable minority concentrations, suggesting the presence of a serious loss mechanism associated with the minority species. This may be a consequence of the large magnetic field ripple in Alcator-C. At high densities, minority temperatures were even lower, but strongly elevated minority temperatures are not expected, because of the efficient collisional coupling of the absorbed RF power to the bulk plasma. The minority temperature was never

sufficiently high to collisionally couple large amounts of power to electrons. In this regime, magnetic field ripple losses of the minority species may be neglected as compared with collisional equilibration on bulk deuterium ions.

To determine the net power deposited to deuterium, existing numerical codes were used to calculate the RF absorption, mode conversion, and collisional deposition in the presence of severe minority losses. It was found that mode conversion plays a significant but not a dominant role in the scaling of deposited power with density. As expected, the deposition of power on deuterium becomes significantly more efficient at high density, offering no clear explanation for the rapidly decreasing ion temperature increase with increasing density. In particular, it is not necessary to generate a strongly elevated minority temperature to achieve efficient absorption of RF power at high density. However, the deposition calculations do offer an explanation for the results of the experimental minority concentration scan. It was found that mode conversion becomes dominant at high concentration, resulting in significantly reduced power deposited on deuterium. This mode conversion behavior is attributed to the inability to produce an elevated minority tail at high minority concentration.

To further investigate the results of the experimental density scan, the deuterium power balance was studied in more detail using the ONETWO transport code. It was found that the dominant loss mechanism for the deuterium is thermal conduction, which increases with density to values significantly above neoclassical predictions at high density. After accounting for losses associated with the minority species, it was found that the unfavorable density scaling of incremental confinement observed in the experiment could quite reasonably be attributed to the behavior of the ion thermal conduction. Since the inferred ion thermal conduction during the Ohmic and RF heated parts of the discharge were in very good agreement, there is no need to postulate the existence of other loss mechanisms, such as a large increase in the previously insignificant convection power.

For relatively low plasma densities, the heating efficiency was limited by poor confinement of the hydrogen minority, with the most severe loss channel being due to toroidal-field ripple-trapping. At high plasma densities, RF power absorption and deposition was relatively efficient, but heating was limited by severe losses associated with anomalous ion

thermal conduction. This ion anomaly may have been caused by η_i-modes, which may have been suppressed in previous Ohmic plasmas by means of pellet injection. These results suggest that future auxiliary heating experiments in high-density, high-magnetic-field plasmas (such as Alcator C-Mod, MTX (Microwave Tokamak Experiment), or CIT (Compact Ignition Tokamak)) be performed in conjunction with pellet injection.

ACKNOWLEDGEMENTS

The authors wish to thank the Alcator C operating team and technical staff for their invaluable contributions to this work. In particular, we wish to thank R. L. Watterson and E. J. Rollins for providing data from the Thomson scattering diagnostic, and S. M. Wolfe for providing data from the FIR (Far Infrared) laser interferometer, assisting with the ONETWO code, and giving guidance regarding other modeling techniques. We also wish to thank M. Brambilla, P. L. Colestock, D. N. Smithe, and G. W. Hammett for assistance with their various modeling codes, and W. W. Pfeiffer and R. Stockdale for allowing us to use the ONETWO code. This work was supported by the United States Department of Energy, Contract No. DE-AC02-78ET-51013.

References and Footnotes

* Current address: Fusion Energy Division, Oak Ridge National Laboratory, Oak Ridge, Tennessee

† Current address: Plasma Physics Group, Saha Institute of Nuclear Physics, Gidhan Nagar, Calcutta India

[1] D. G. Swanson, *Phys. Fluids* **28**:9, 2645 (1985).

[2] J. Adam, *Plasma Phys.* **29**:4, 443 (1987).

[3] M. P. J. Gaudreau, M. Sansone, B. D. Blackwell, F. Knowlton, D. Lavoie, C. Holtjer, B. Abbanat, Medium Power ICRF Results on the Alcator A Tokamak, in *Proceedings of the 4th Topical Conference on Radio Frequency Plasma Heating*, (University of Texas, Austin, TX, 1981) p. A9-1

[4] M. Porkolab, B. Blackwell, P. Bonoli, D. Griffin S. Knowlton, B. Lloyd, J. Moody, J. J. Schuss, Y. Takase, S. Texter, R. Watterson, C. Fiore, M. Foord, R. Gandy, C. Gomez, R. Granetz, M. Greenwald, D. Gwinn, B. Labombard, B. Lipschultz, H. Manning, E. Marmar, S. McCool, J. Moreno, A. Pachtamn ,D. Pappas, R. Parker, P. Pribyl, J. Rice, T. Shepard, J. Terry, S. Wolfe, D. Yates, K.I. Chen, S.C. Luckhardt, M.J. Mayberry, G. Bekefi, R. Rohatgi, Plasma Physics and Controlled Nuclear Fusion Research, (IAEA, Vienna, 1985) Vol.1, p. 463.

[5] H.L. Manning, J. Terry, B. Lipschultz, B. Labombard, B. Blackwell, C. Fiore, M. Foord, E. Marmar, J. Moody, R. Parker, M. Porkolab, J. Rice ,*Nucl. Fus.* **26** (1986), 1665.

[6] H. L. Manning, *VUV Study of Impurity Generation During ICRF Heating Experiments on the Alcator C Tokamak*, Ph.D. Thesis, Harvard University (May, 1986).

[7] J. D. Moody, M. Porkolab, *Phys. Fluids* **B 8**, 1675 (1989).

[8] M. Greenwald, D. Gwinn, S. Milora, J. Parker, R. Parker, S. Wolfe, M. Besen, F. Camacho, S. Fairfax, C. Fiore, M. Foord, R. Gandy, C. Gomez, R. Granetz, B. Labombard, B. Lipschultz, B. Lloyd, E. Marmar, S. McCool, D. Pappas, R. Petrasso, P.

Pribyl, J. Rice, D. Schuresko, Y. Takase, J. Terry, R. Watterson, *Phys. Rev. Let.*, Vol. 53, No. 4, 23 July, 1984.

[9] R. R. Parker, M. Greenwald, S. C. Luckhardt, E. S. Marmar, M. Porkolab, S. M. Wolfe, *Nucl. Fusion* **25**:9, 1127 (1985).

[10] S. M. Wolfe, M. Greenwald, R. Gandy, R. Grantez, C. Gomez, D. Gwinn, B. Lipschultz, S. McCool, E. Marmar, J. Parker, R. R. Parker, J. Rice, *Nucl. Fusion* **26**:3, 329 (1986).

[11] W. Pfeiffer, F. B. Marcus, C. J. Armentrant, G. L. Johns, T. W. Petrie, R. E. Stockdale, *Nucl. Fusion* **25**, 655 (1985).

[12] M. Porkolab, *Phys. Lett.* **22**, 427 (1966).

[13] B. Coppi, M. N. Rosenbluth, R. Z. Sagdeev, *Phys. Fluids* **10**:3, 582 (1967).

[14] M. Porkolab, *Nucl. Fusion* **8**, 29 (1968).

[15] T. Antonsen, B. Coppi, R. Englade, *Nucl. Fusion* **19**, 641 (1979).

[16] H. Biglari, P. H. Diamond, P. W. Terry, *Phys. Rev. Lett.* **60**:3, 200 (1988).

[17] T. D. Shepard, *Fast Wave Ion Cyclotron Resonance Heating Experiments on the Alcator C Tokamak*, Ph.D. Thesis, Massachusetts Institute of Technology (1988).

[18] R. L. Watterson, F. Tambini, M. Besen, J. Bosco, G. Chihoski, N. Pierce, S. McCool, *Bull. Am. Phys. Soc.* **30**, 1497 (1985).

[19] EQUIPE TFR, ICRF Heating and Antenna Coupling Studies in TFR, *Proceedings of the 3rd Joint Varenna-Grenoble International Symposium - Heating in Toroidal Plasmas*, (Grenoble, France, 22-26 March 1982) **I**, p. 225.

[20] T. H. Stix, *Nucl. Fusion* **15**, 737 (1975).

[21] D. P. Schissel, *High Energy Ion Depletion in the Charge Exchange Spectrum of Alcator C*, MS Thesis, MIT (1982).

[22] M. E. Foord, E. S. Marmar, J. L. Terry, *Rev. Sci. Instrum.* **53**, 1407 (1982).

[23] M. Brambilla, *Nucl. Fusion* **28**:4, 549 (1988).

[24] D. N. Smithe, P. L. Colestock, R. J. Kashuba, T. Kammash, *Nucl. Fusion* **27**:8, 1319 (1987).

[25] D. Smithe, P. Colestock, T. Kammash, R. Kashuba, *Phys. Rev. Lett.* **60**:9, 801 (1988).

[26] P. L. Colestock, R. J. Kashuba, *Nucl. Fusion* **23**:6, 763 (1983).

[27] G. W. Hammett, *Fast Ion Studies of Ion Cyclotron Heating in the PLT Tokamak* Princeton University, Ph.D. Thesis (1986).

[28] C. S. Chang, F. L. Hinton, *Phys. Fluids* **25**, 1493 (1982).

[29] F. L. Hinton, R. D. Hazeltine, *Rev. Mod. Phys.* **48**:2, 239 (1976).

TABLE I. TYPICAL PLASMA PARAMETERS

Parameter	Alcator	ICRF
R_0 (cm)	64	64
a (cm)	16.5	12.5
B_0 (T)	5–13	12
I_P (kA)	50–800	140–410
$\bar{n}_e$ (10^{20} m^{-3})	0.3–20	0.8–5
T_e (keV)	1–3	1.5–2.5
T_i (keV)	0.5–1.5	1–1.3
τ_E (ms)	5–50	5–25
P_{OH} (MW)	0.1–1.5	0.2–1

TABLE II. PARAMETERS FOR RISING DENSITY

Parameter	Ohmic	RF
T_D	900 eV	1300 eV
I_P	154 kA	154 kA
q_a	9.5	9.5
V_R	1.5 V	2.15 V
P_{OH}	230 kW	330 kW
P_{RF}	0 kW	300 kW
$\bar{n}_e$	0.84×10^{20} m^{-3}	1.35×10^{20} m^{-3}
n_{e0}	1.0×10^{20} m^{-3}	2.0×10^{20} m^{-3}
η_H	$\sim 0.5\%$	—
Z_{eff}	2.2	3.5
τ_E	7.7 ms	5.2 ms[a]

[a] Assumes 100% RF absorption.

TABLE III. PARAMETERS FOR STEADY DENSITY

Parameter	Ohmic	RF
T_D	970 eV	1145 eV
I_P	160 kA	160 kA
q_a	9.25	9.25
V_R	1.5 V	1.8 V
P_{OH}	240 kW	290 kW
P_{RF}	0 kW	220 kW
$\bar{n}_e$	$1.0 \times 10^{20}\,m^{-3}$	$1.0 \times 10^{20}\,m^{-3}$
n_{e0}	$1.3 \times 10^{20}\,m^{-3}$	$1.3 \times 10^{20}\,m^{-3}$
η_H	$\sim 0.5\%$	—
Z_{eff}	1.9	2.6
τ_E	8.6 ms	4.3 ms[a]

[a] Assumes 100% RF absorption.

TABLE IV. PARAMETERS FOR RADIAL CX SCAN

Parameter	Ohmic	RF
T_D	1100 eV	1240 ± 15 eV
I_P	165 kA	165 kA
q_a	8.9	8.9
V_R	1.6 V	1.9 ± 0.3 V
P_{OH}	265 ± 5 kW	320 ± 60 kW
P_{RF}	0 kW	250 ± 40 kW
$\bar{n}_e$	$1.4 \times 10^{20}\,m^{-3}$	$1.2 \times 10^{20}\,m^{-3}$
τ_E	12.5 ± 2.5 ms	6 ± 3 ms[a]

[a] Assumes 100% RF absorption.

TABLE V. PARAMETERS FOR CONCENTRATION SCAN

Parameter	Ohmic	RF
T_D	1250 ± 50 eV	—
I_P	200 kA	200 kA
q_a	7.5	7.5
V_R	1.65 ± 0.05 V	2.15 ± 0.15 V
P_{OH}	330 ± 10 kW	430 ± 30 kW
P_{RF}	0 kW	290 ± 80 kW
$\bar{n}_e$	1.25×10^{20} m^{-3}	1.45×10^{20} m^{-3}
τ_E	14 ± 3 ms	8 ± 1 ms[a]

[a] Assumes 100% RF absorption.

FIGURE CAPTIONS

[1] Two different antennas were used to couple ICRF power to the Alcator C plasmas. The low-field-side launch antenna (a) is a simple center-tapped loop, while the two-side launch antenna (b) is a self-resonant structure with an asymmetric tap point chosen to provide a matched load to the feed line. Each antenna consists of two conductors spaced toroidally and fed in phase.

[2] Plasma parameters for a discharge with density increasing during the RF power injection. Shown are central deuterium temperature T_D (from charge-exchange diagnostic), plasma current I_P, line-averaged density $\bar{n}_e$, and resistive loop voltage V_R. Other parameters for this discharge are shown in Table II.

[3] Plasma parameters for a discharge with density steady during the RF power injection. Shown are central deuterium temperature T_D (from neutron diagnostic), plasma current I_P, line-averaged density $\bar{n}_e$, and resistive loop voltage V_R. Other parameters for this discharge are shown in Table III.

[4] Thomson scattering data showing no significant electron heating during RF heating. Parameters for this discharge were similar to those in Table IV.

[5] Hydrogen-minority tail temperature as a function of minor radius, determined by vertically scanning the charge-exchange diagnostic. Other parameters for this scan are listed in Table IV.

[6] Results from hydrogen minority concentration scan. The central hydrogen tail temperature is shown in (a) and the increase in central deuterium temperature is shown in (b). The best deuterium heating was always obtained at the lowest possible minority concentration. The results are normalized to RF power here because there was a $\pm 27\%$ variation in RF power during the scan. Other parameters for this scan are shown in Table V.

[7] Typical deuterium charge-exchange spectrum showing heating but no non-thermal tail. T_D before RF = 0.88 keV, T_D during 220 kW RF = 1.07 keV.

[8] Raw deuterium heating data for the entire data base. Shown is the increase in central deuterium temperature $\Delta T_D \equiv T_D(0)|_{\rm RF} - T_D(0)|_{\rm OH}$ as a function of line-averaged density $\bar{n}_e$. The RF power corresponding to the highest values of ΔT_D was constant at $P_{\rm RF} \sim 300$ kW for $0.8 \leq \bar{n}_e \lesssim 2 \times 10^{20}\,{\rm m}^{-3}$, then decreasing to $P_{\rm RF} \sim 175$ kW at $\bar{n}_e \sim 5 \times 10^{20}\,{\rm m}^{-3}$.

[9] Energy confinement time $\tau_E \equiv W/P$ as a function of line-averaged density during both Ohmic and RF-heated portions of the discharge (a) and incremental energy confinement time $\tau_{\rm inc} \equiv \Delta W/\Delta P$ as a function of line-averaged density (b).

[10] $Z_{\rm eff}$ determined from resistive loop voltage as a function of line-averaged electron density.

[11] Power balance diagram. The various energy channels and notation that will be used to refer to them are identified in this diagram.

[12] Power deposition analysis for a 6-point density scan (a). The total coupled RF power $P_{\rm RF} = 220$ kW is absorbed via hydrogen fundamental (P_H) or deuterium second harmonic (P_D) cyclotron absorption, or is mode-converted ($P_{\rm MC}$) to the ion Bernstein wave. After accounting for losses, the thermalization of the minority tail yields a collisional-exchange power P_{HD} from hydrogen to deuterium. The net power transferred to the deuterium is $P_{\rm Net} = P_D + P_{HD}$. The peak-to-volume-average profile shape for the net power deposited to deuterium is shown in (b).

[13] Power deposition analysis for simulated minority-concentration scan.

[14] The neoclassical anomaly factor $W_{\rm neo}$, necessary to balance the terms in Eq. 1, is shown as a function of time for three different densities. For case (a) density increased from $\bar{n}_e = 1.35 \times 10^{20}\,{\rm m}^{-3}$ to $\bar{n}_e = 1.53 \times 10^{20}\,{\rm m}^{-3}$ during RF power injection, case (b) had a decrease from $\bar{n}_e = 1.8 \times 10^{20}\,{\rm m}^{-3}$ to $\bar{n}_e = 1.6 \times 10^{20}\,{\rm m}^{-3}$, and

for case (c) the density was nearly constant, decreasing from $\bar{n}_e = 2.95 \times 10^{20}\,\mathrm{m}^{-3}$ to $\bar{n}_e = 2.8 \times 10^{20}\,\mathrm{m}^{-3}$ during RF injection. The power-balance calculation was performed using three different models for the RF deposition: $P_{\mathrm{dep}} = P_{\mathrm{RF}}$ (all of the launched RF power deposited to deuterium), $P_{\mathrm{dep}} = 0$ (none of the launched RF power deposited to deuterium), and $P_{\mathrm{dep}} = P_{\mathrm{net}}$ (from the calculations described herein).

[15] The neoclassical anomaly factor is shown as a function of density before and during the RF power injection, for all 44 shots that were analyzed (a). Bold error bars include uncertainty in experimental measurements of electron and ion temperatures and electron density, while other error bars include variation in nominal experimentally measured values before and during the RF power injection. The values of the actual thermal conductivity κ_D at $r = a/2$ are shown in (b).

[16] Total heating power to deuterium, including electron-ion collisional exchange P_{eD} is shown as a function of line-averaged density.

LOW-FIELD-SIDE LAUNCH ANTENNA

(a)

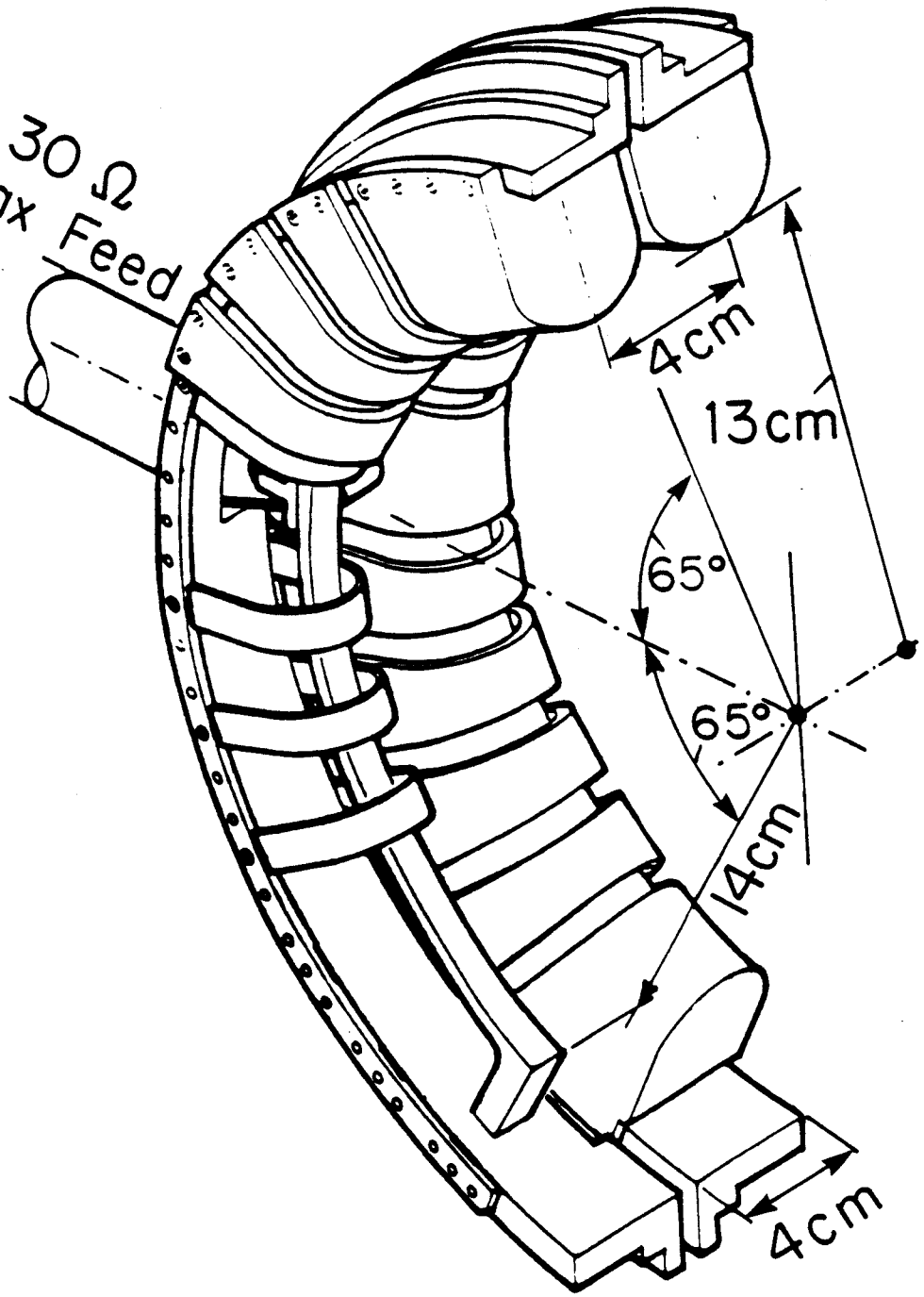

Figure 1(a)

TWO-SIDE LAUNCH ANTENNA

(b)

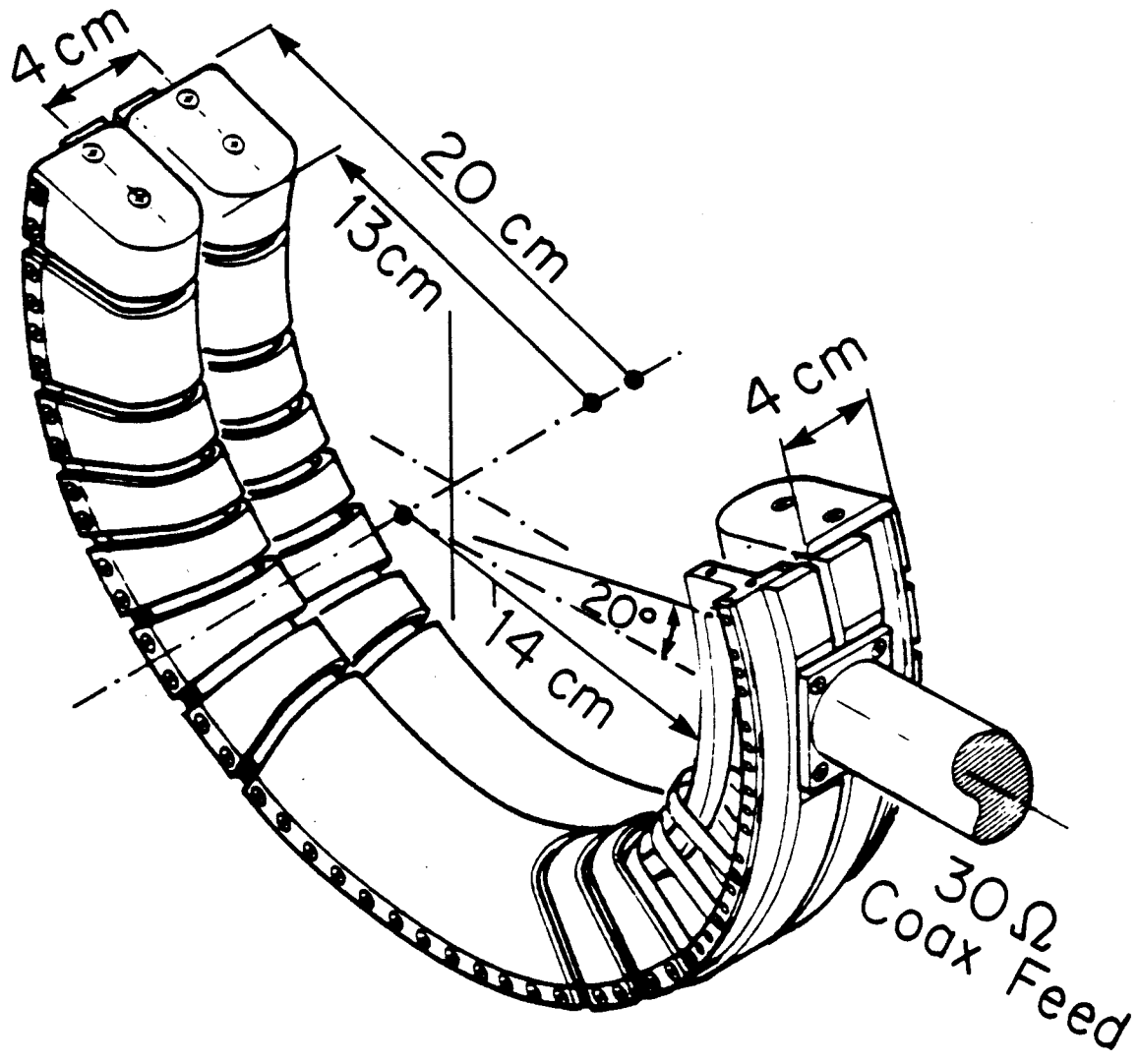

Figure 1(b)

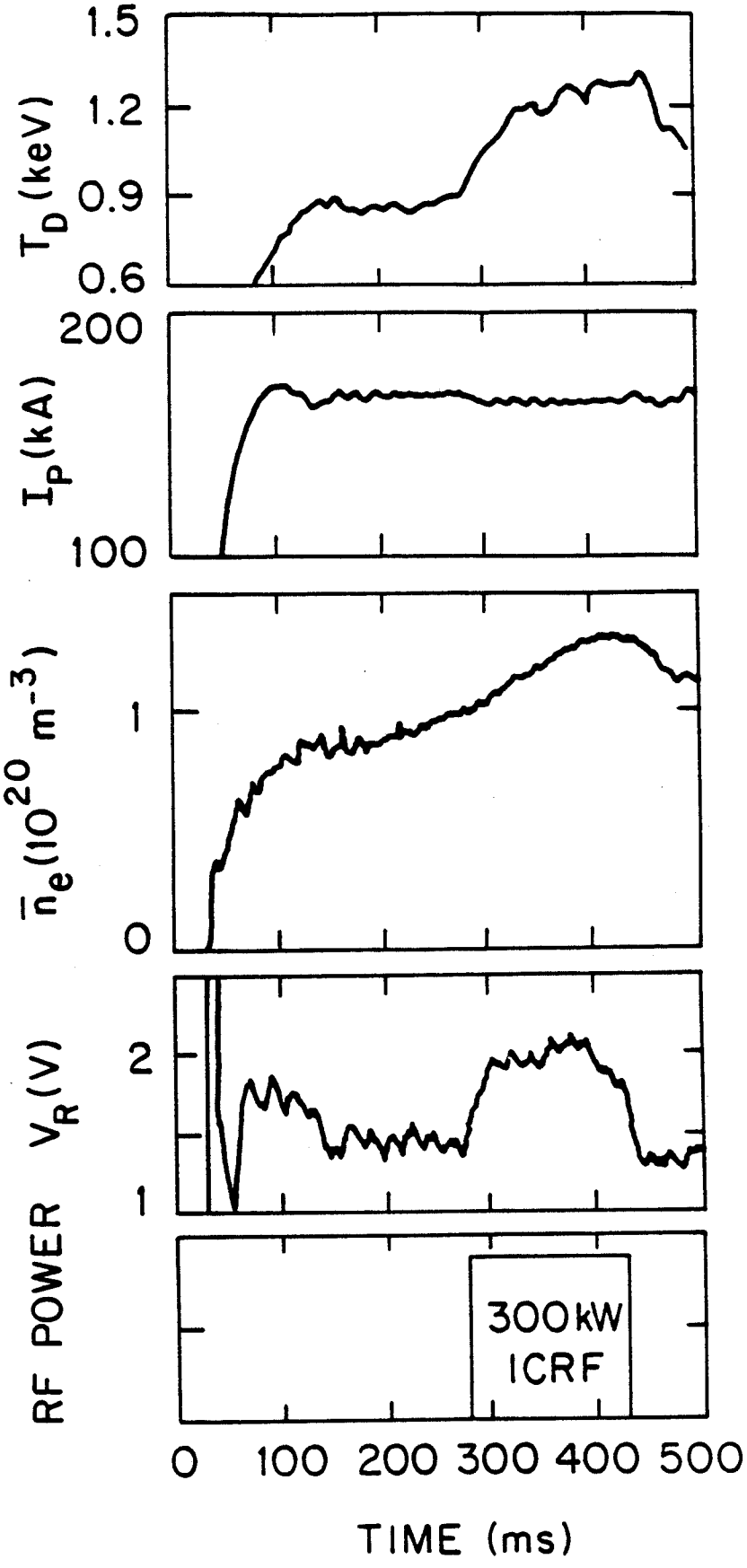
1.5
1.2
0.9
0.6
T_D (keV)
200
100
I_p (kA)
1
0
$\bar{n}_e (10^{20}\ m^{-3})$
2
1
V_R (V)
RF POWER
300 kW
ICRF
0
100
200
300
400
500
TIME (ms)

Figure 2

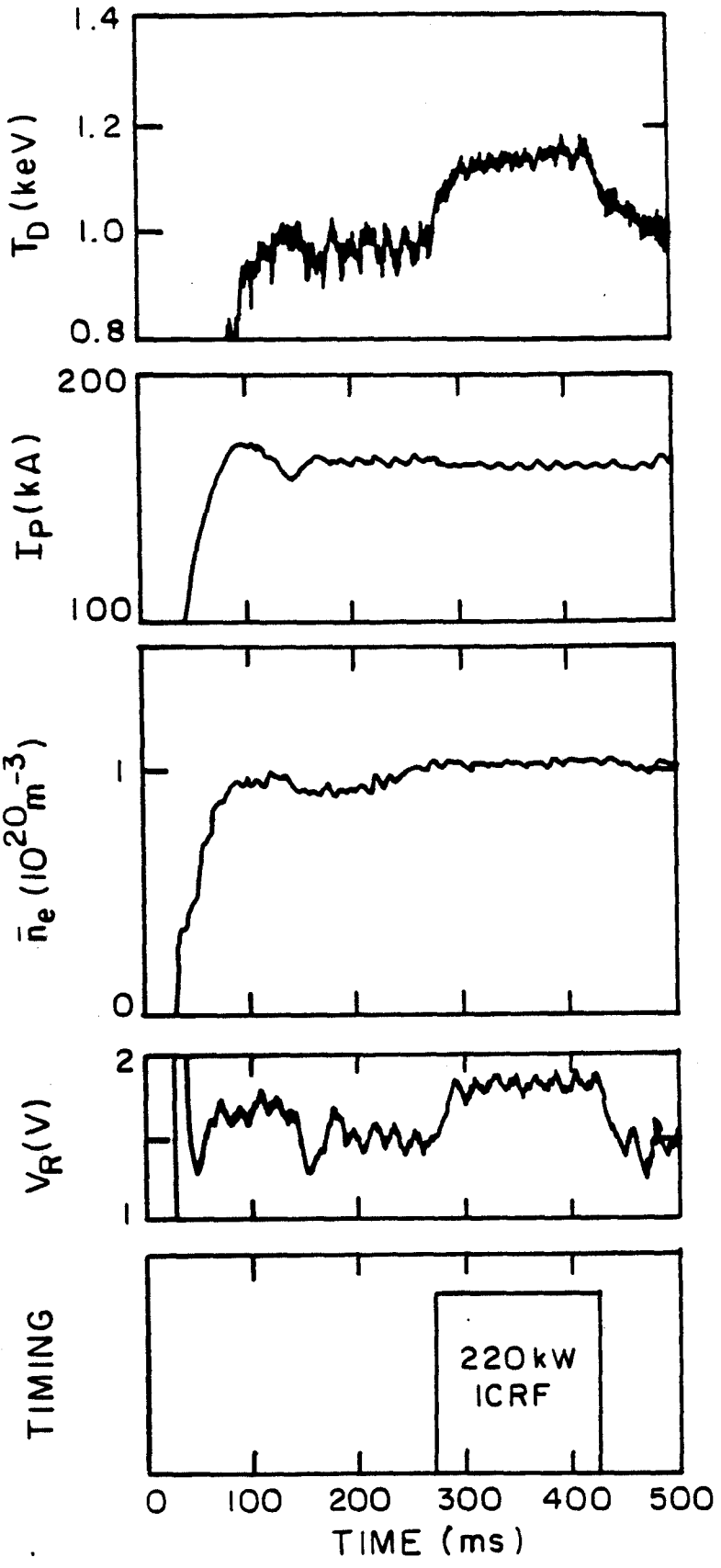
1.4
1.2
1.0
0.8
T_D (keV)
200
100
I_P (kA)
$\bar{n}_e$ ($10^{20}m^{-3}$)
1
0
2
1
V_R (V)
TIMING
220 kW
ICRF
0
100
200
300
400
500
TIME (ms)

Figure 3

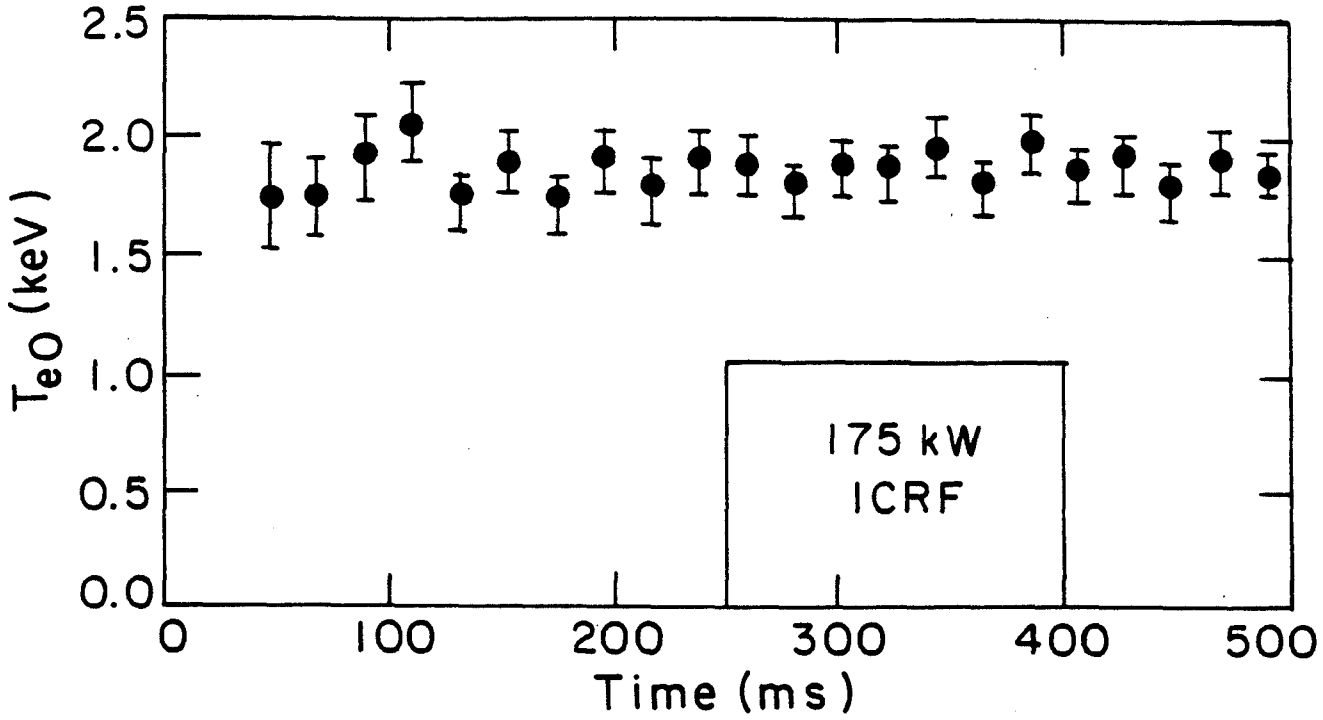
2.5
2.0
1.5
1.0
0.5
0.0
T_{eO} (keV)
175 kW
ICRF
0
100
200
300
400
500
Time (ms)

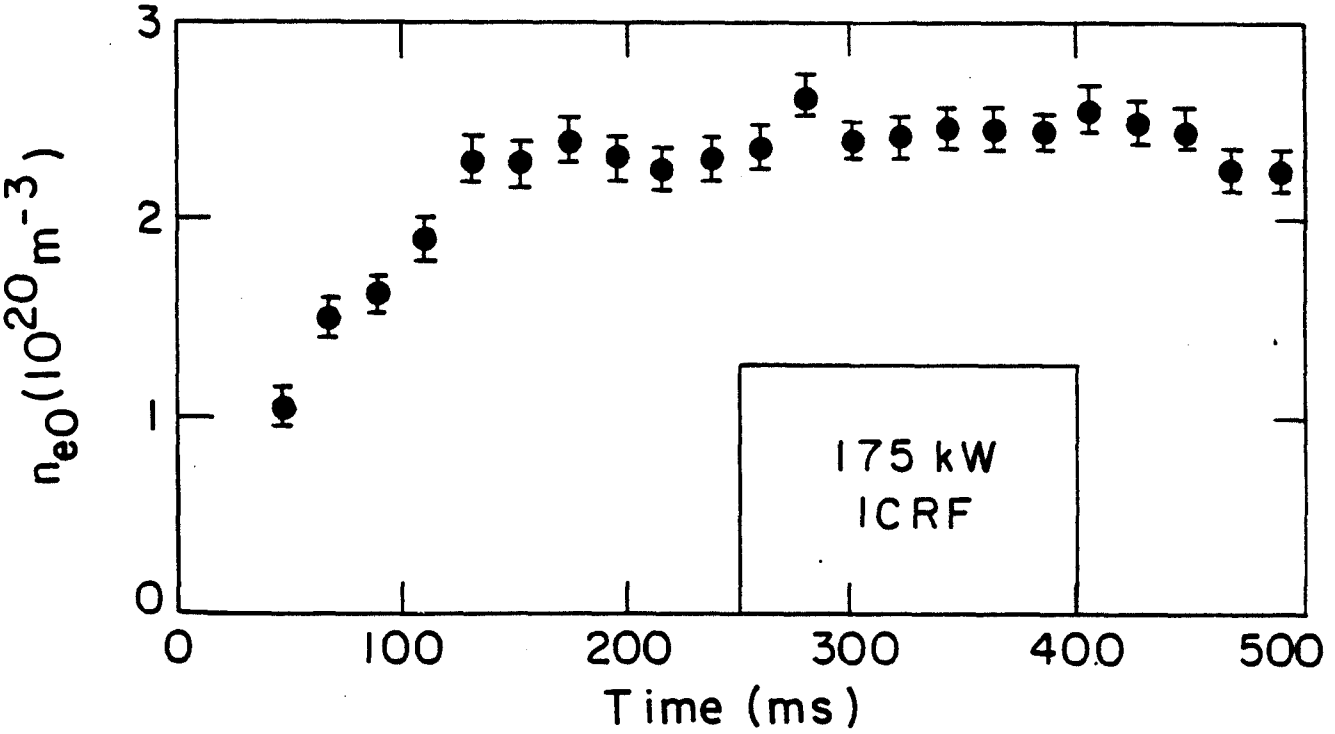
3
2
1
0
$n_{eO}(10^{20} m^{-3})$
175 kW
ICRF
0
100
200
300
400
500
Time (ms)

Figure 4

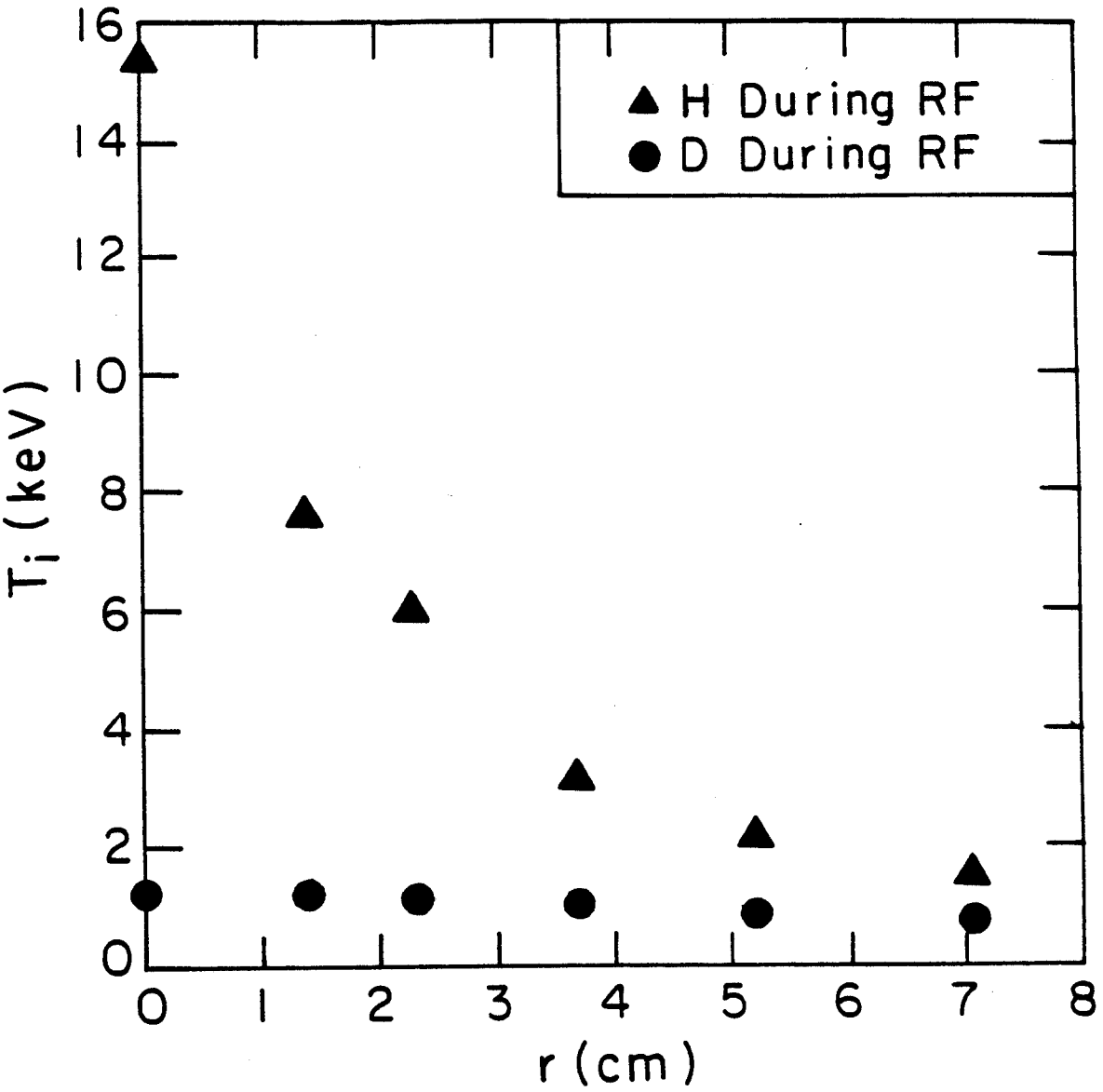

Figure 5

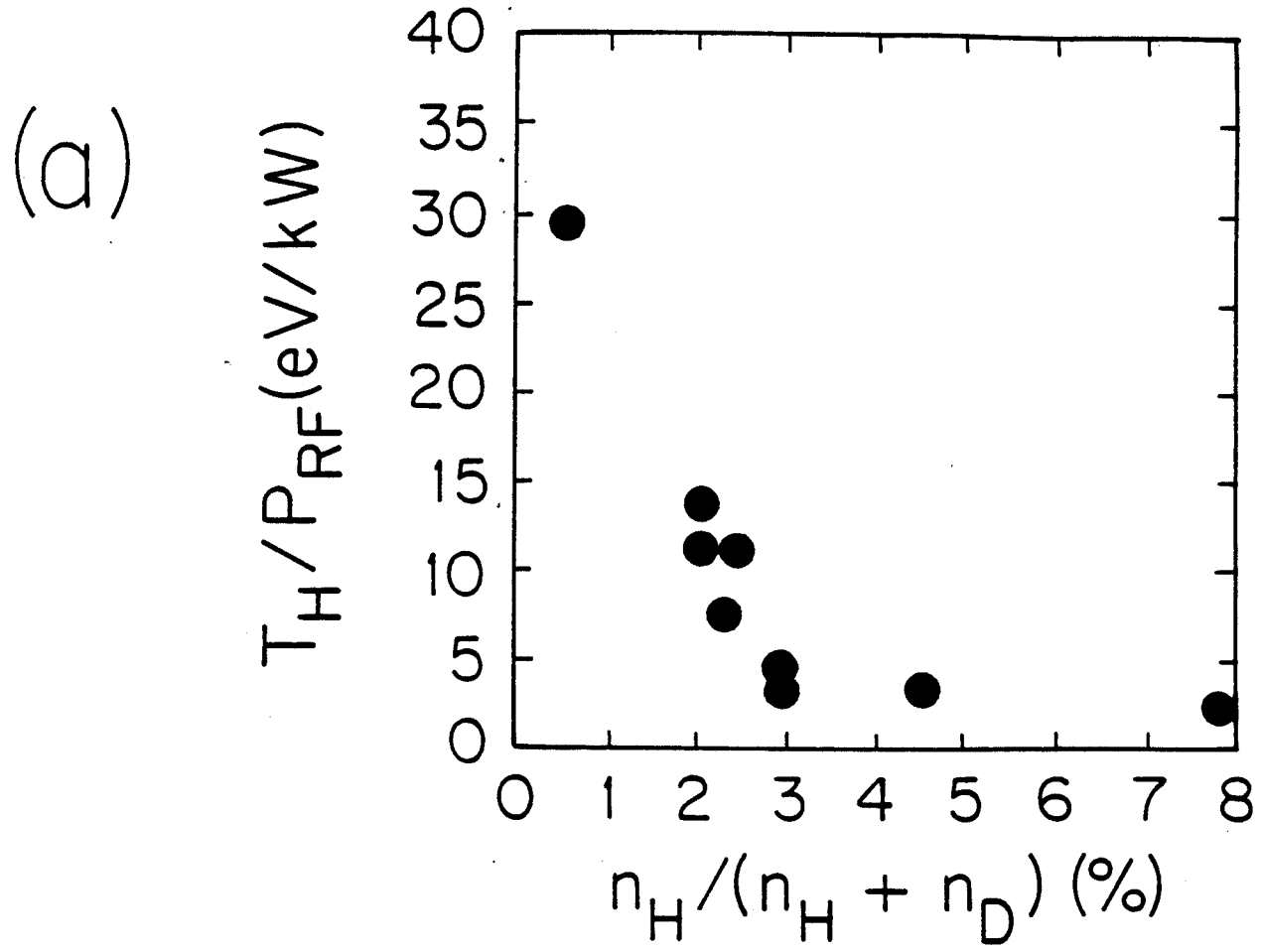
(a)
T_H / P_{RF} (eV/kW)
40
35
30
25
20
15
10
5
0
0 1 2 3 4 5 6 7 8
$n_H/(n_H + n_D)$ (%)

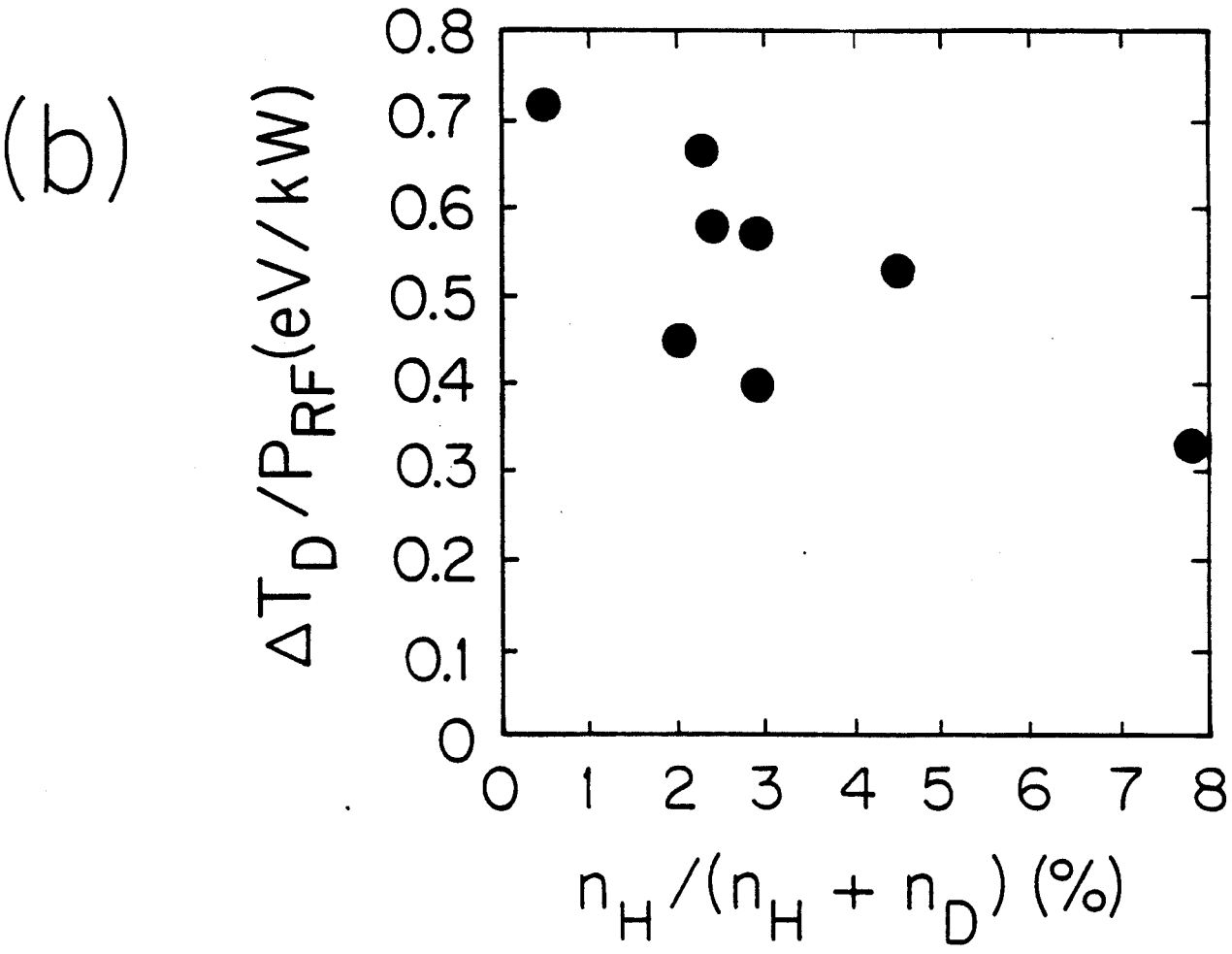
(b)
$\Delta T_D / P_{RF}$ (eV/kW)
0.8
0.7
0.6
0.5
0.4
0.3
0.2
0.1
0
0 1 2 3 4 5 6 7 8
$n_H/(n_H + n_D)$ (%)

Figure 6

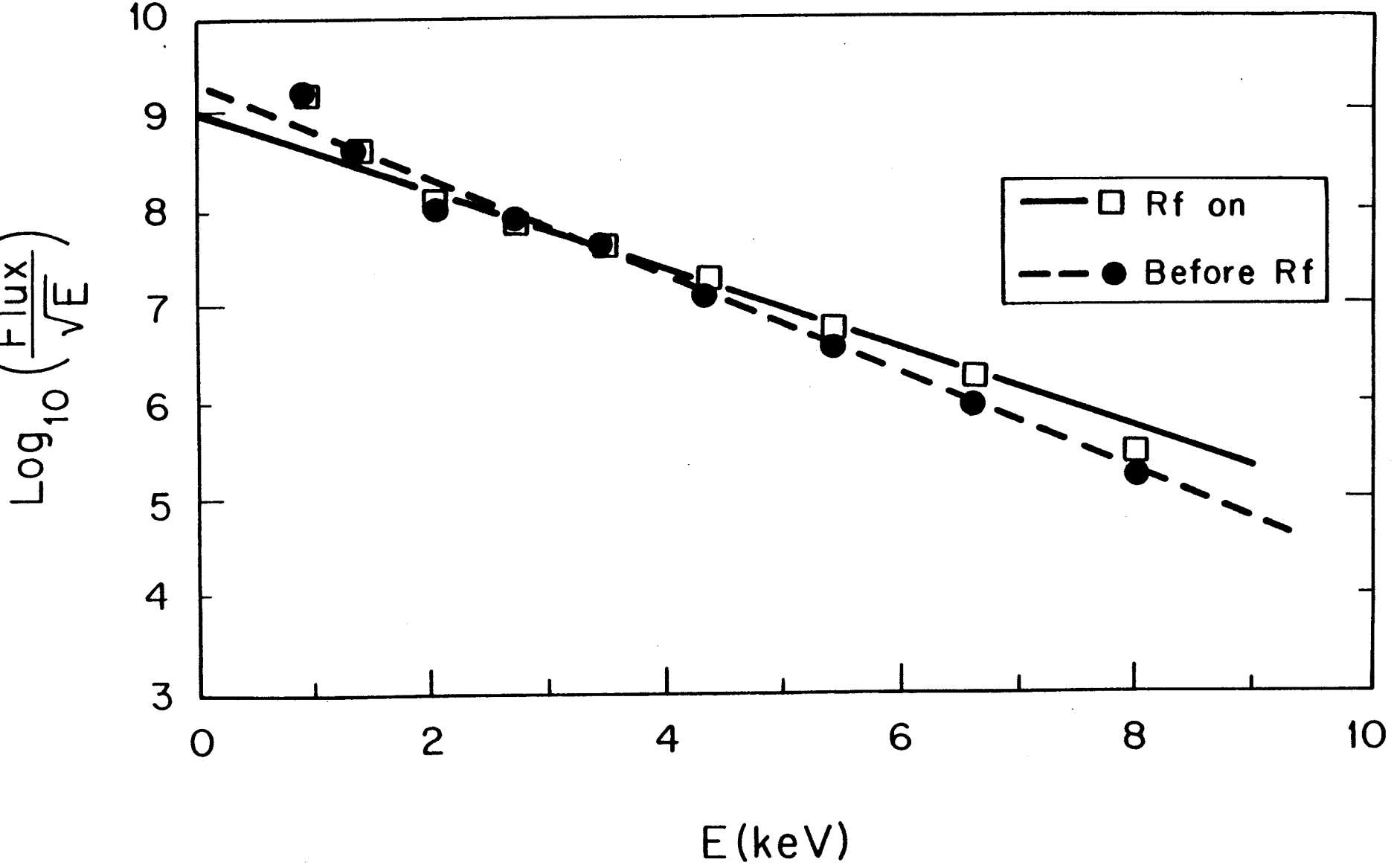
10
9
8
7
6
5
4
3
0
2
4
6
8
10
$Log_{10}\left(\frac{Flux}{\sqrt{E}}\right)$
E(keV)
Rf on
Before Rf

Figure 7

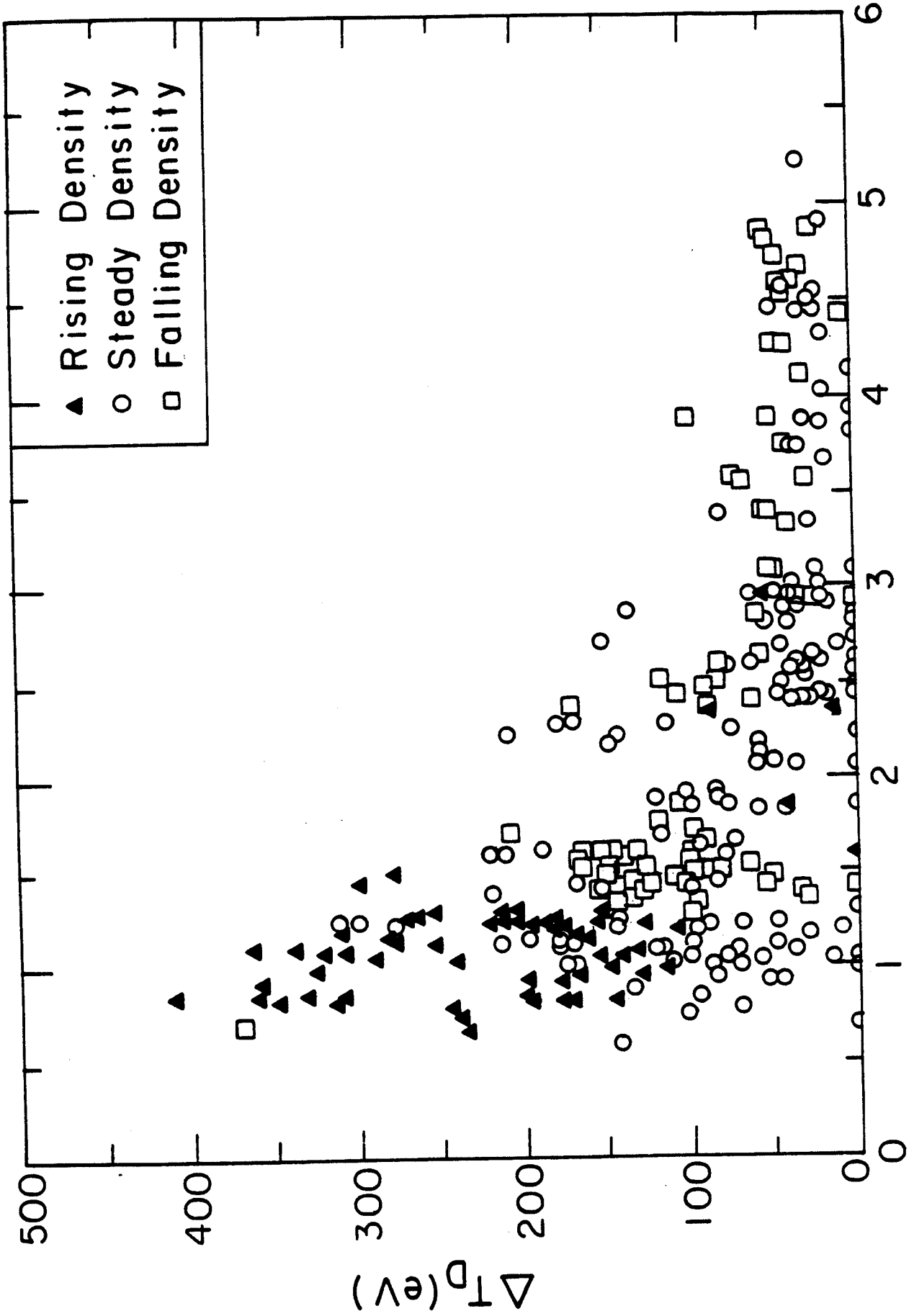
Rising Density
Steady Density
Falling Density
ΔT_D(eV)
$\bar{n}_e$ (10^{20} m^{-3})
0
100
200
300
400
500
1
2
3
4
5
6

Figure 8

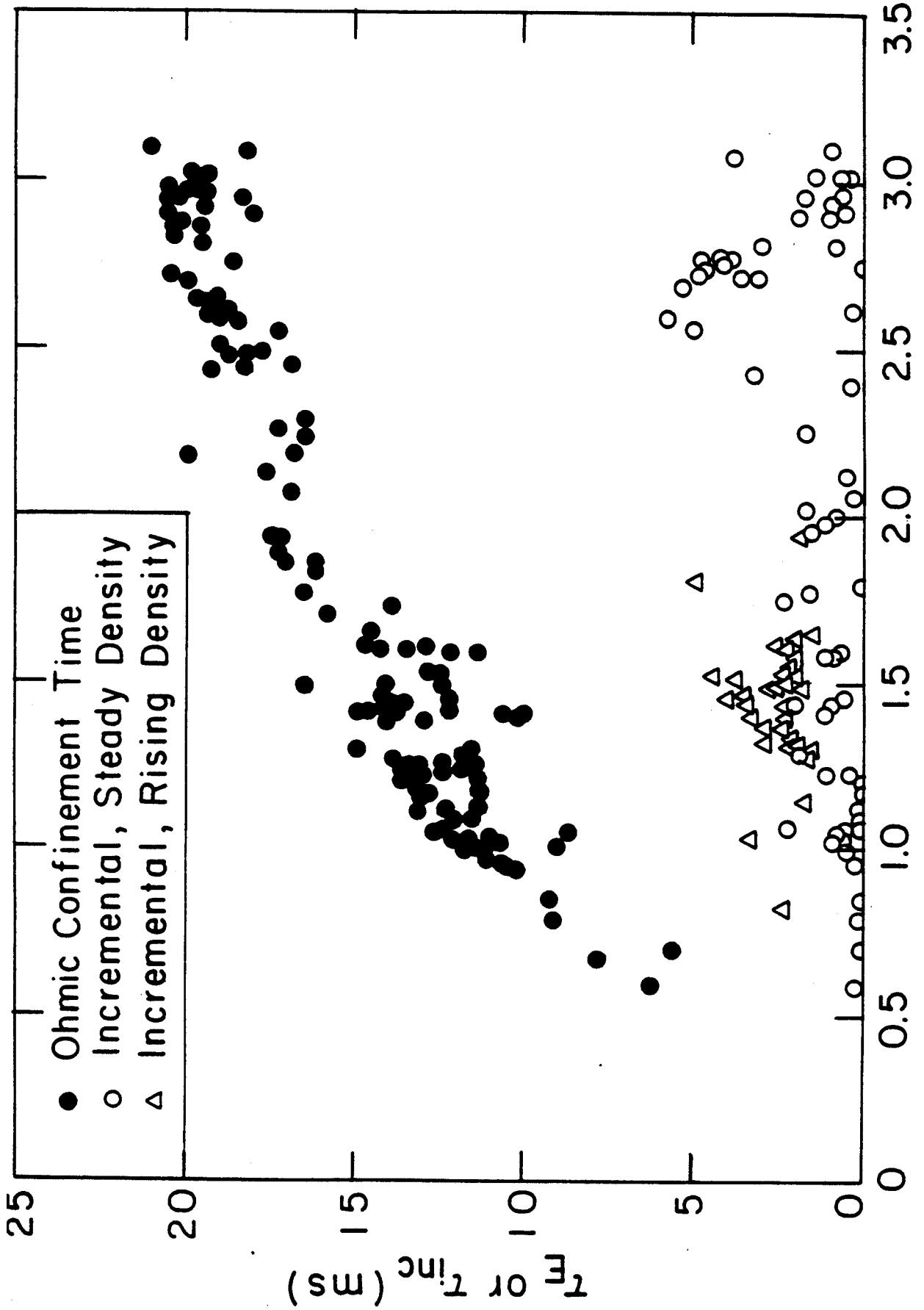
Ohmic Confinement Time
Incremental, Steady Density
Incremental, Rising Density
τ_E or τ_{inc} (ms)
$\bar{n}_e$ (10^{20} m^{-3})
0
5
10
15
20
25
0
0.5
1.0
1.5
2.0
2.5
3.0
3.5

Figure 9(a)

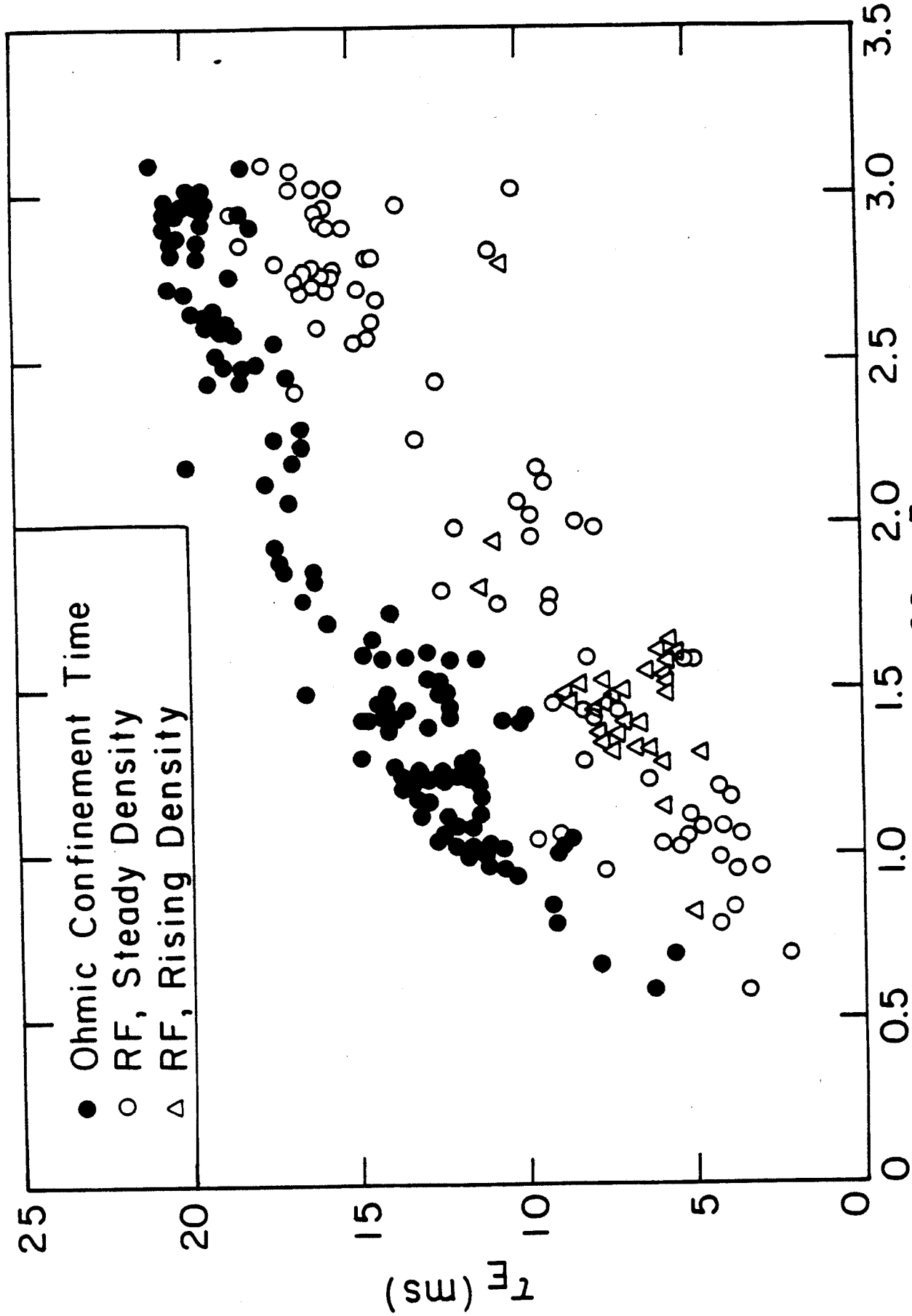
Ohmic Confinement Time
RF, Steady Density
RF, Rising Density
τ_E (ms)
$\bar{n}_e$ (10^{20} m^{-3})
0
5
10
15
20
25
0
0.5
1.0
1.5
2.0
2.5
3.0
3.5

Figure 9(b)

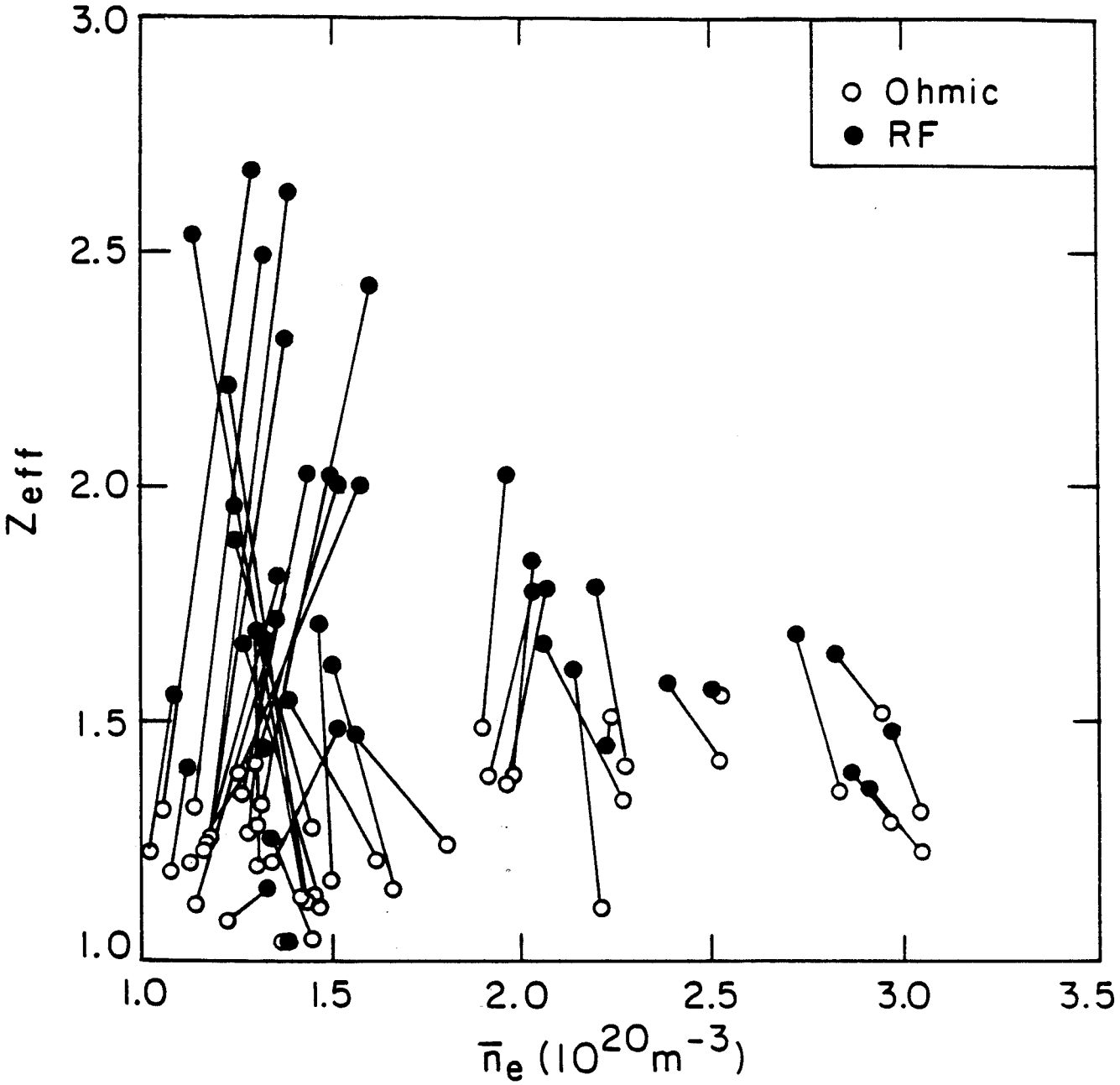

Figure 10

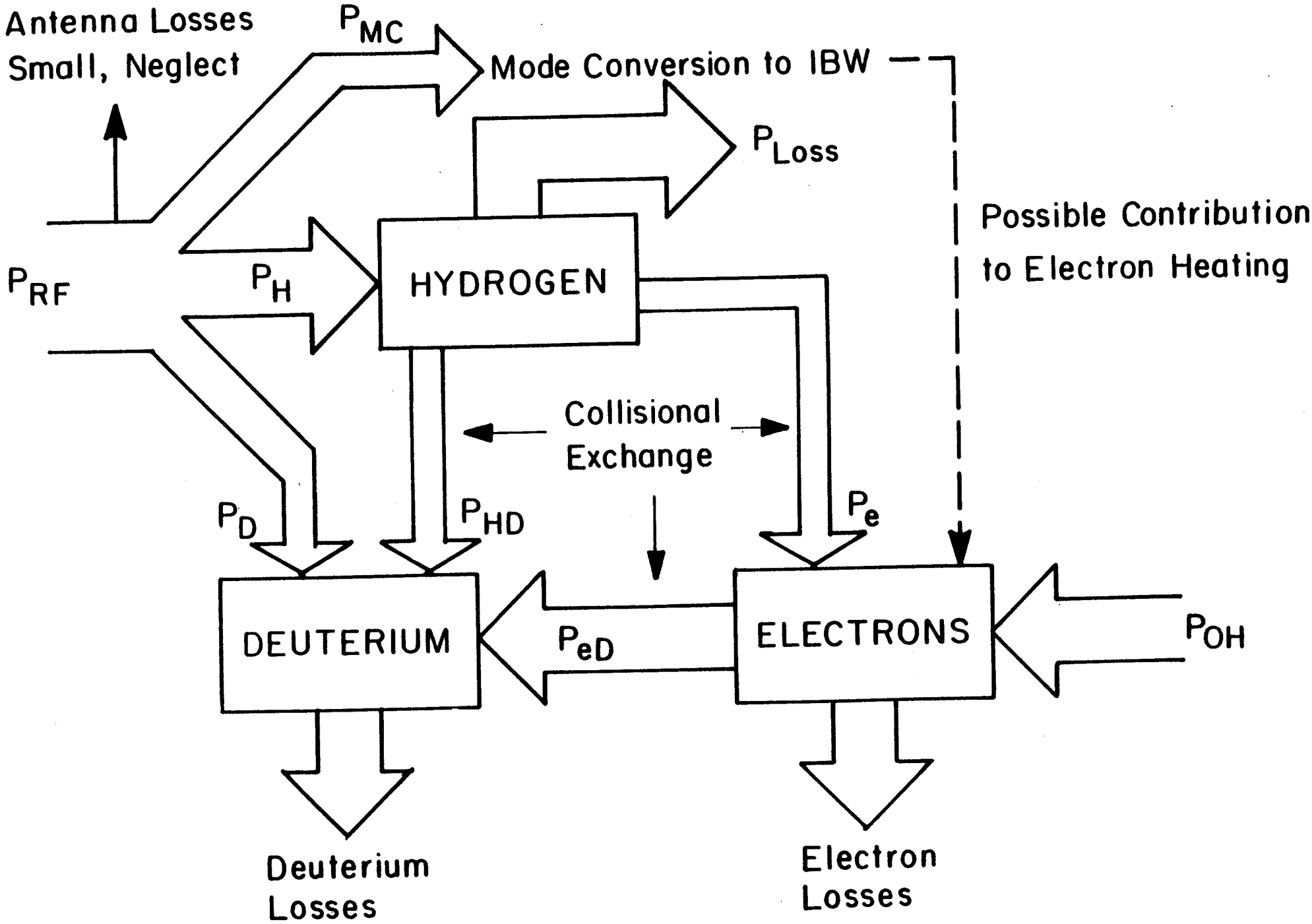
Antenna Losses
Small, Neglect
P_{MC}
Mode Conversion to IBW
P_{Loss}
Possible Contribution
to Electron Heating
P_{RF}
P_H
HYDROGEN
Collisional
Exchange
P_D
P_{HD}
P_e
DEUTERIUM
P_{eD}
ELECTRONS
P_{OH}
Deuterium
Losses
Electron
Losses

Figure 11

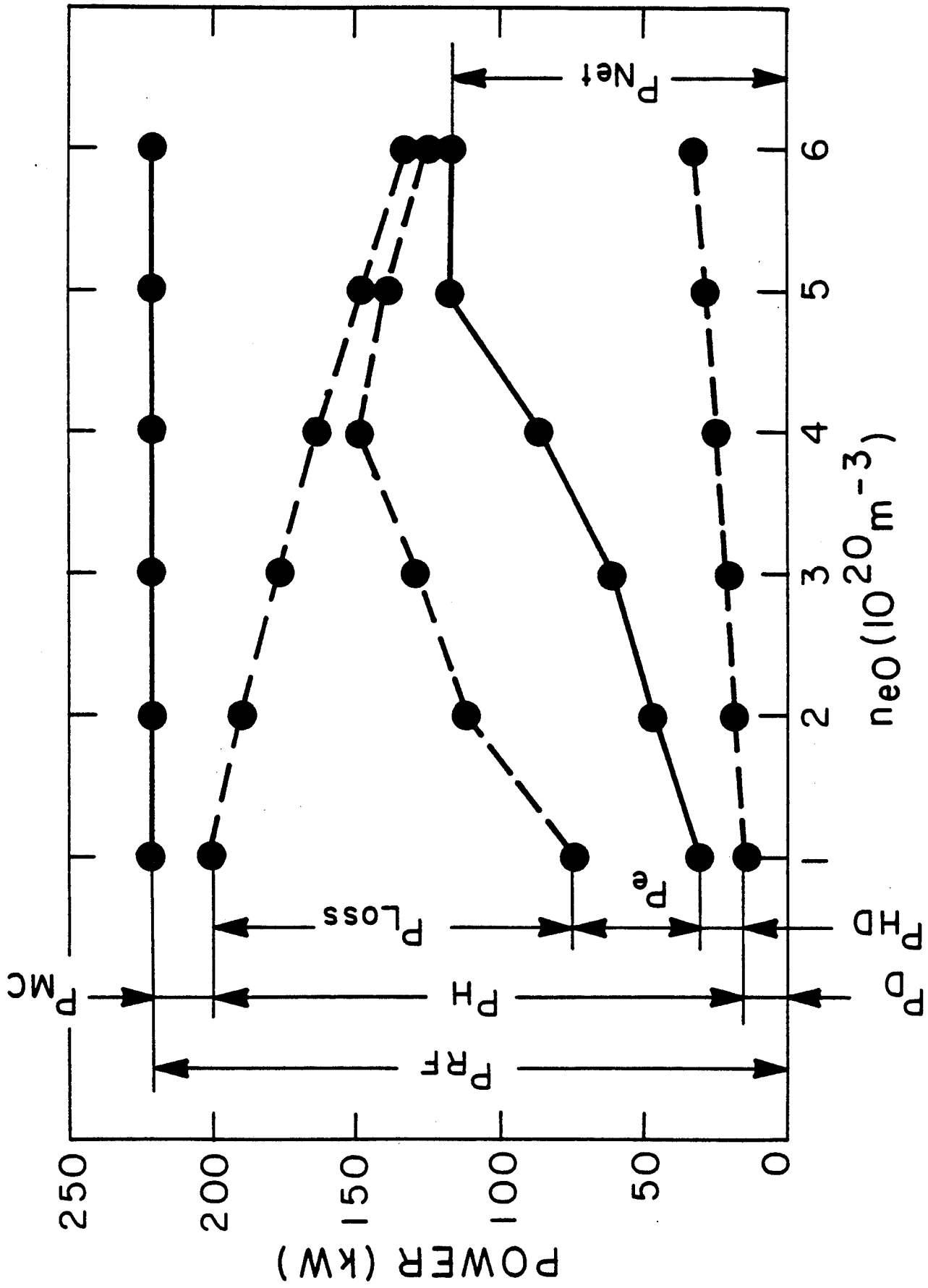
POWER (kW)
250
200
150
100
50
0
$n_{eO}(10^{20}m^{-3})$
1
2
3
4
5
6
P_{Net}
P_{RF}
P_H
P_{MC}
P_{Loss}
P_e
P_{HD}
P_D

Figure 12(a)

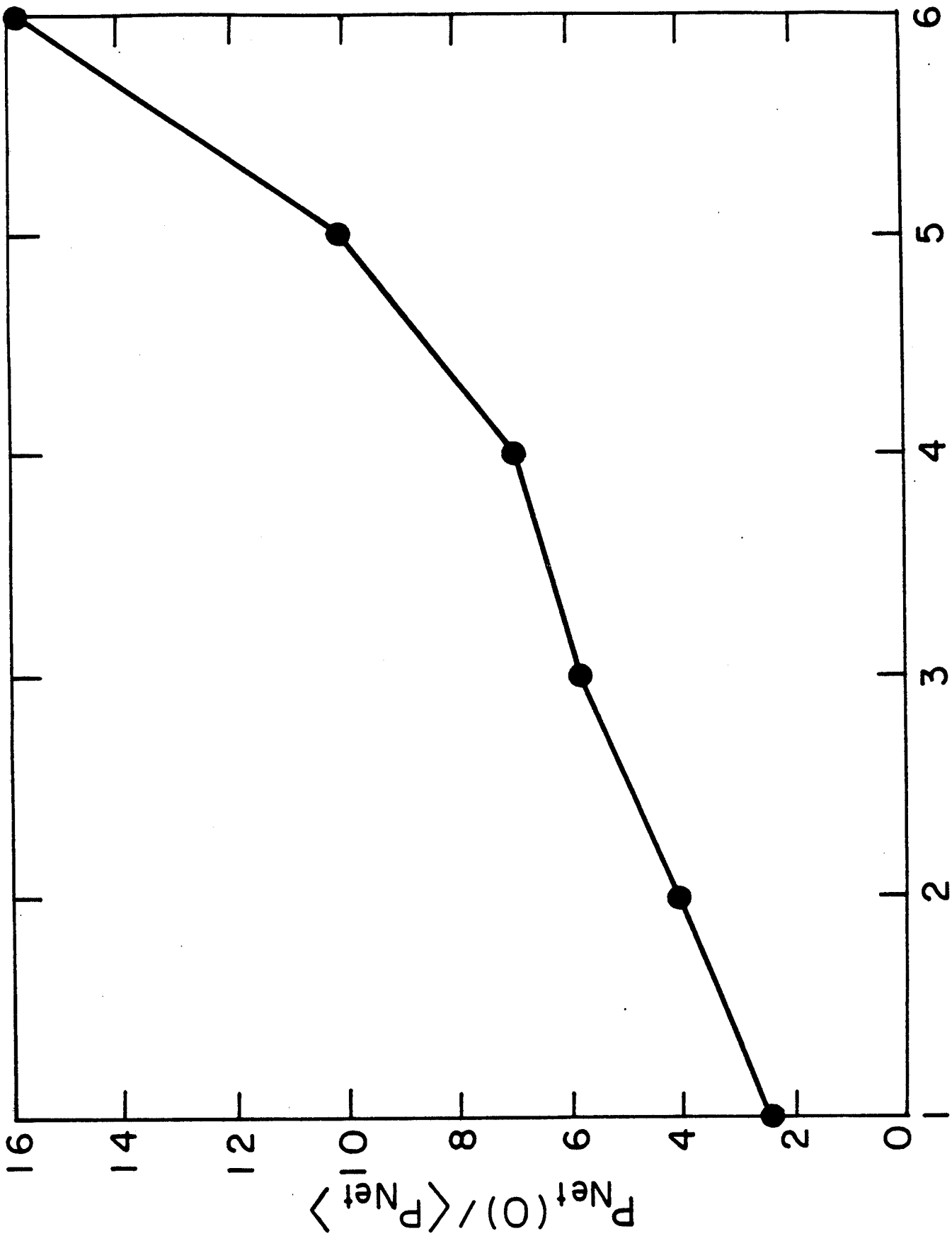

Figure 12(b)

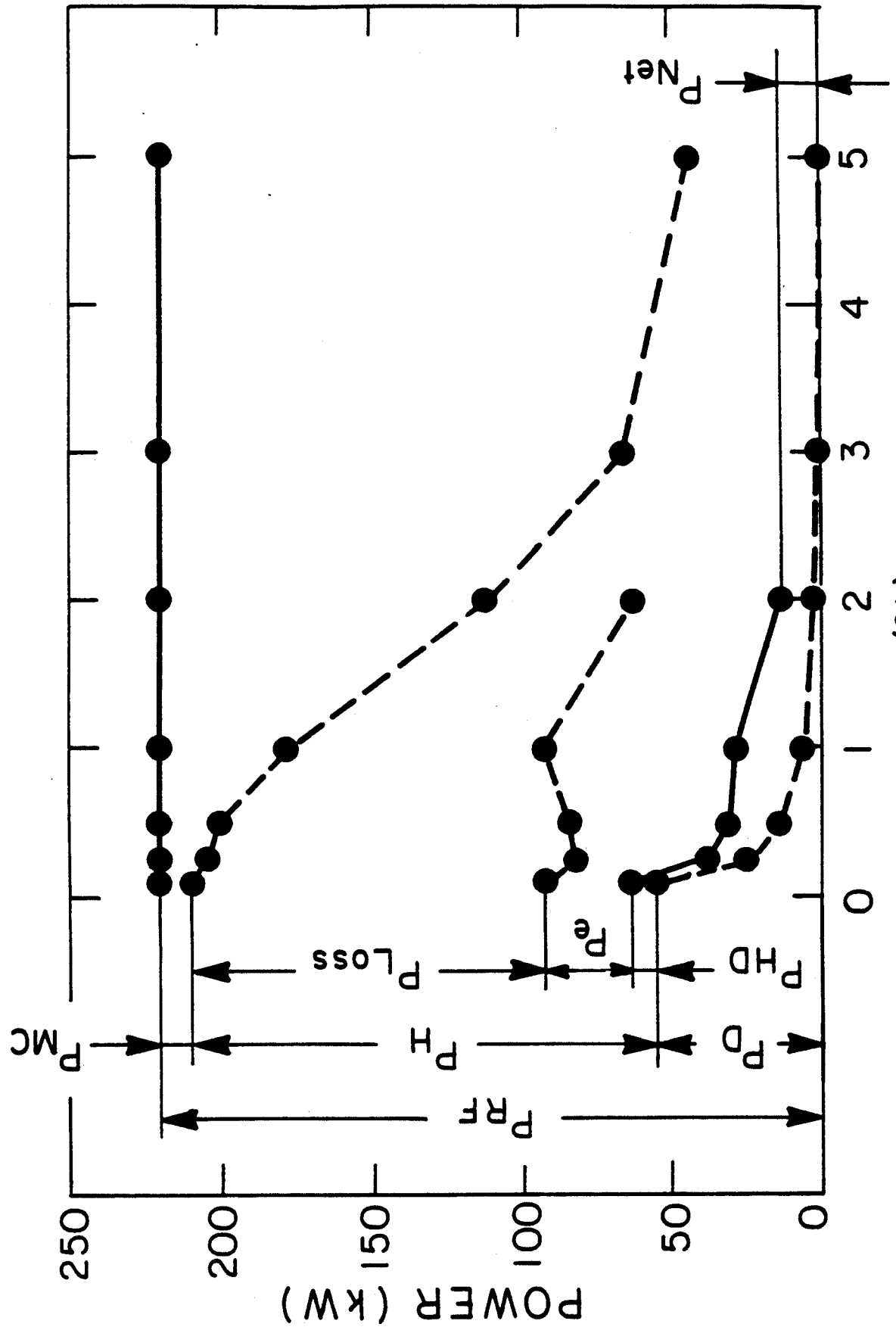
POWER (kW)
250
200
150
100
50
0
P_{RF}
P_{MC}
P_H
P_D
P_{Loss}
P_e
P_{HD}
P_{Net}
0
1
2
3
4
5
η_H (%)

Figure 13

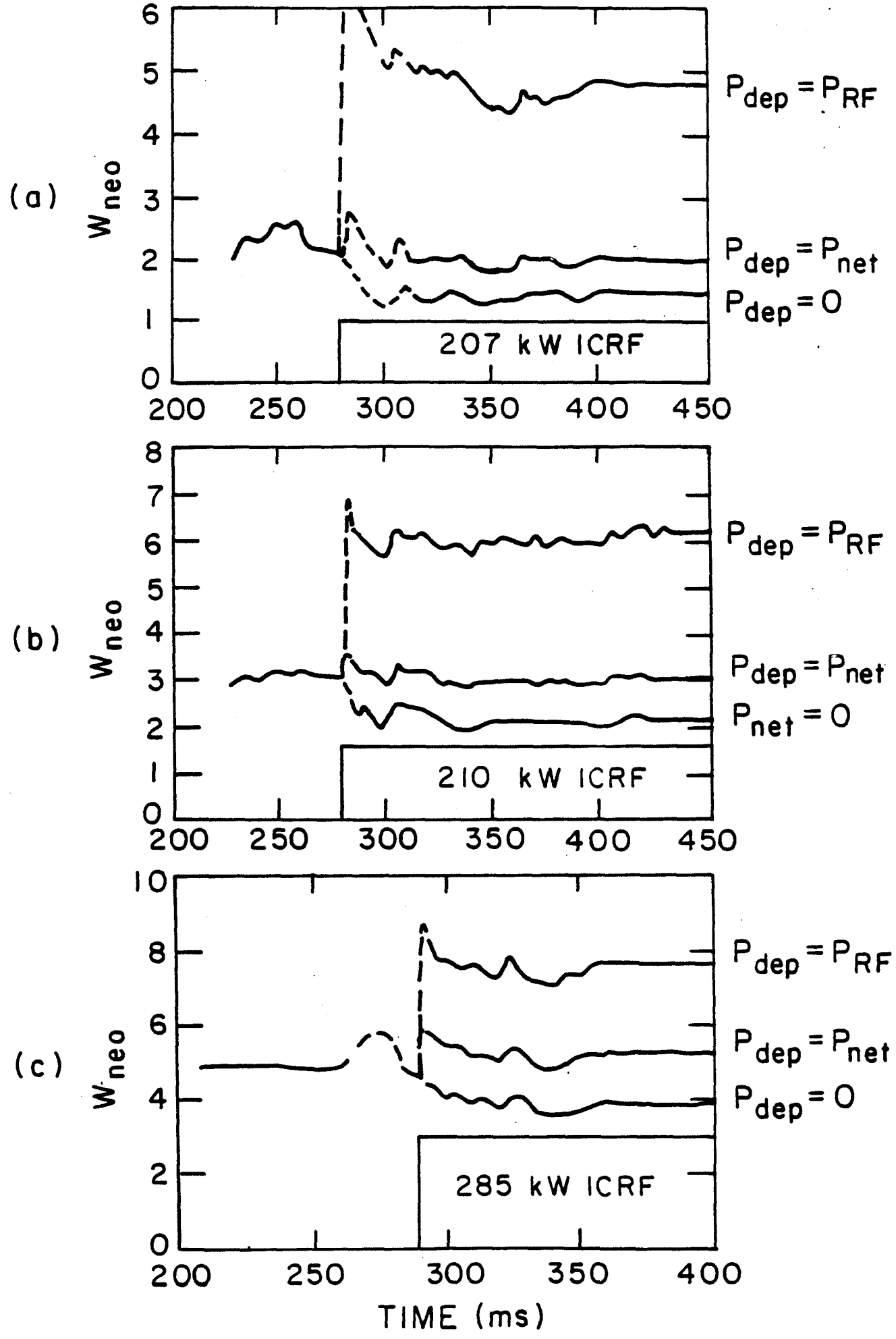
(a)
(b)
(c)
W_{neo}
$P_{dep} = P_{RF}$
$P_{dep} = P_{net}$
$P_{dep} = 0$
$P_{net} = 0$
207 kW ICRF
210 kW ICRF
285 kW ICRF
TIME (ms)

Figure 14

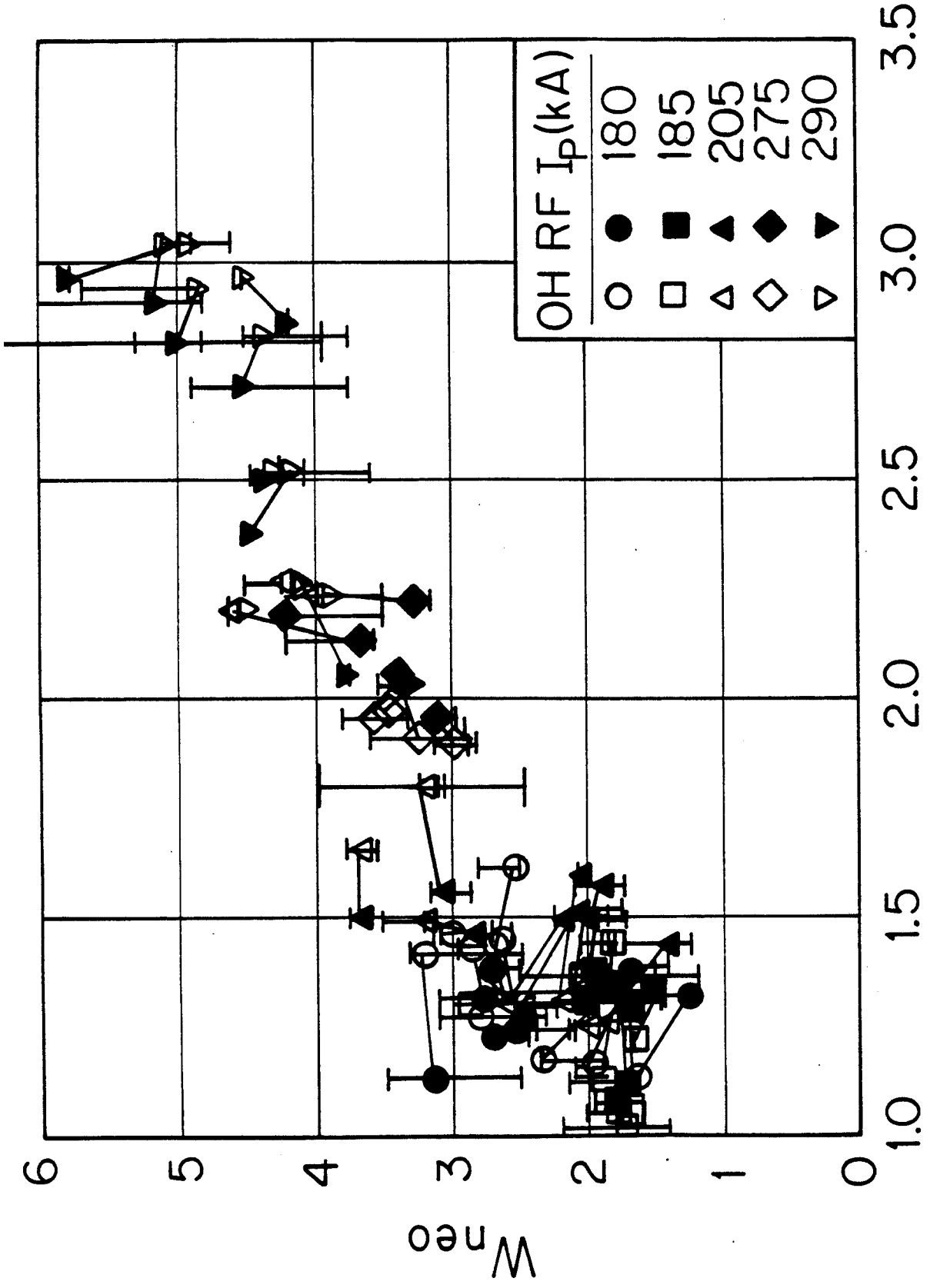
OH RF I_p(kA)
180
185
205
275
290
W_{neo}
$\bar{n}_e(10^{20}\ m^{-3})$
0
1
2
3
4
5
6
1.0
1.5
2.0
2.5
3.0
3.5

Figure 15(a)

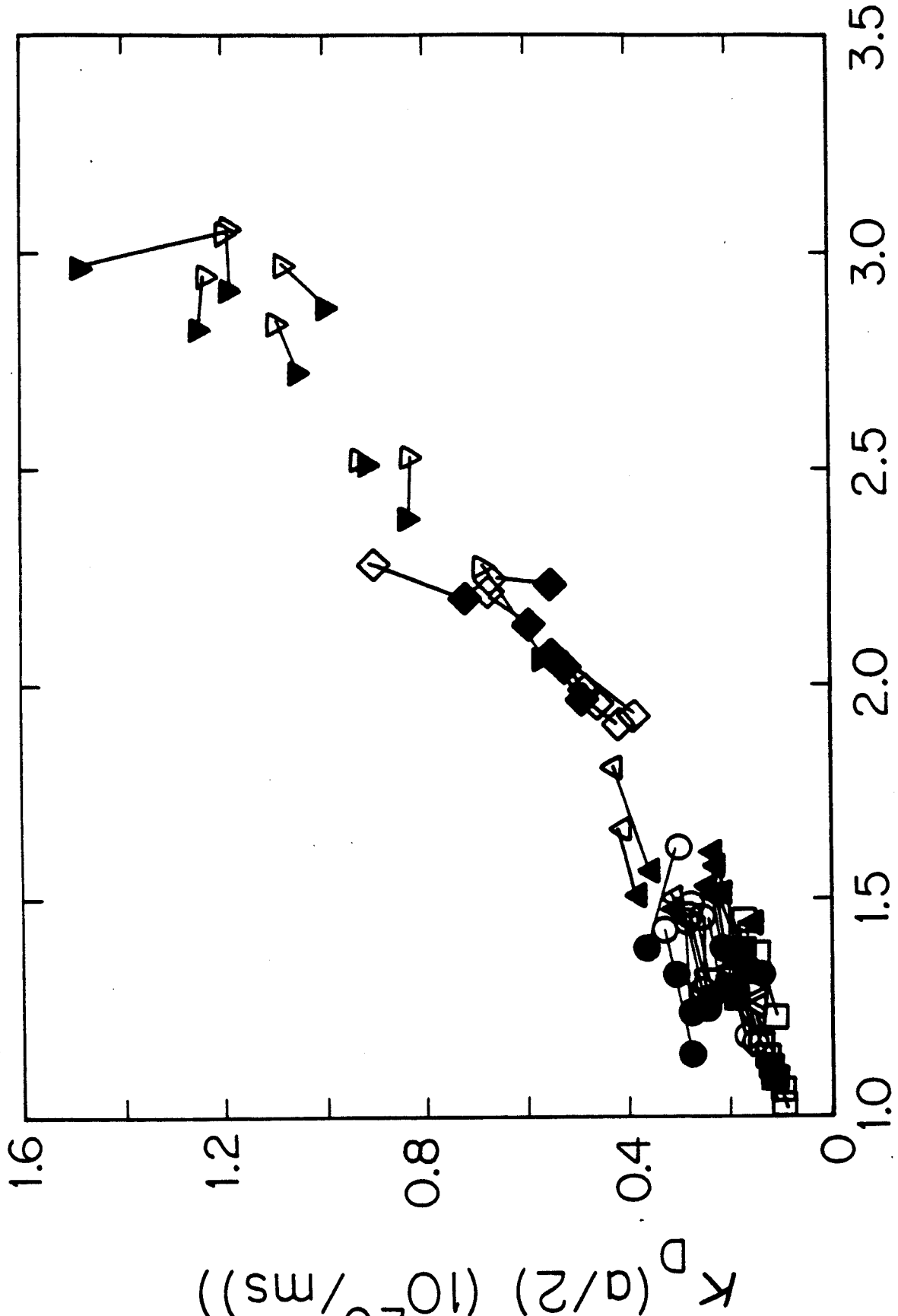

Figure 15(b)

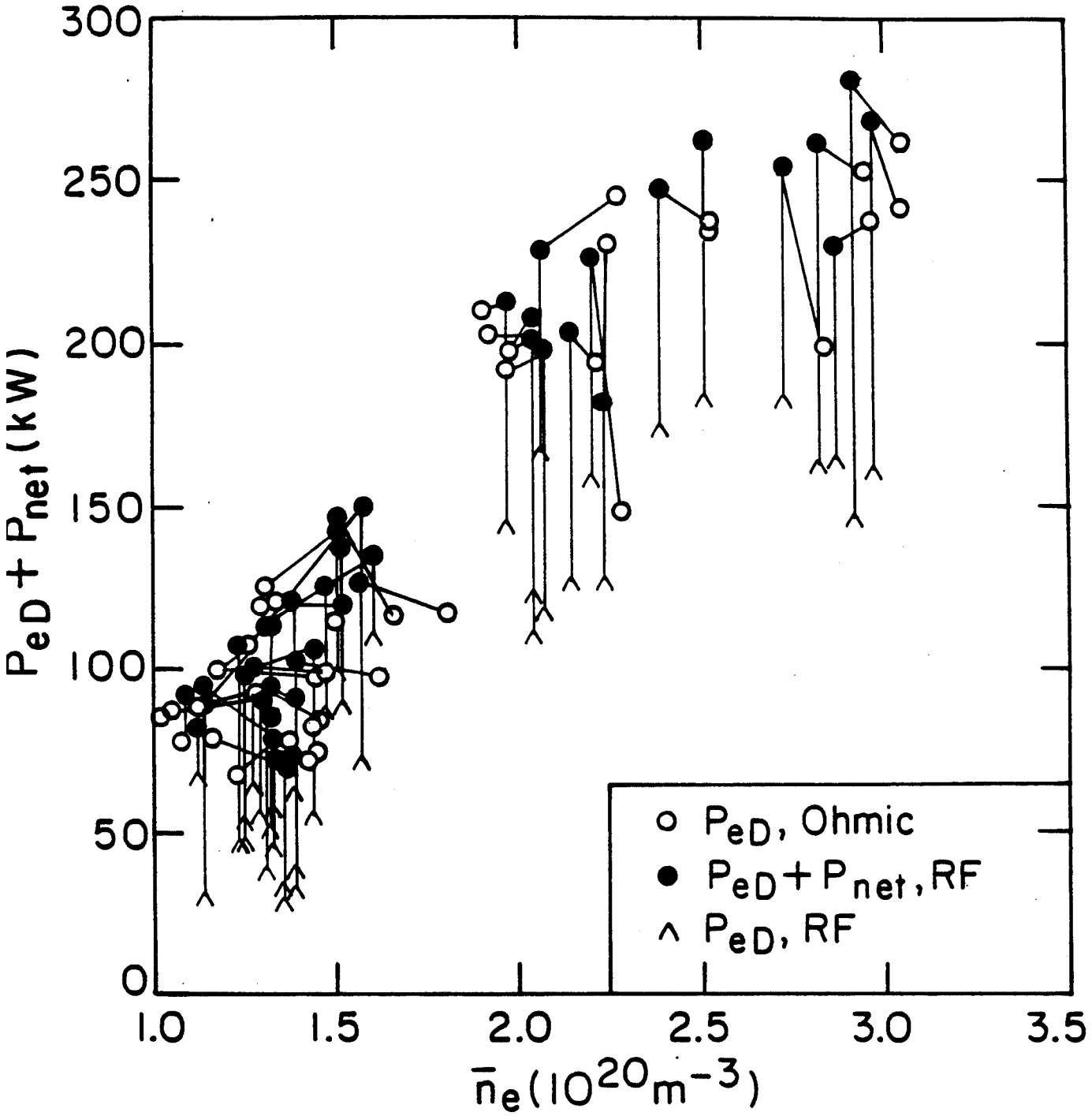
300
250
200
150
100
50
0
$P_{eD} + P_{net}$ (kW)
1.0
1.5
2.0
2.5
3.0
3.5
$\bar{n}_e (10^{20} m^{-3})$
P_{eD}, Ohmic
$P_{eD} + P_{net}$, RF
P_{eD}, RF

Figure 16